

Computation-Efficient Semi-Supervised Learning for ECG-based Cardiovascular Diseases Detection

Rushuang Zhou^{1,3}, Zijun Liu^{1,3}, Lei Clifton⁴, David A. Clifton^{5,6},
Kannie W. Y. Chan^{1,3,7,8}, Yuan-Ting Zhang^{9,10}, Yining Dong^{2,3*}

¹Department of Biomedical Engineering, City University of Hong Kong, Hong Kong, China.

²School of Data Science, City University of Hong Kong, Hong Kong, China.

³Hong Kong Center for Cerebro-Cardiovascular Health Engineering,
Hong Kong Science Park, Hong Kong, China.

⁴Nuffield Department of Population Health, University of Oxford, Oxford, UK.

⁵Department of Engineering Science, University of Oxford, Oxford, UK.

⁶Oxford-Suzhou Institute of Advanced Research, Suzhou, China.

⁷Russell H. Morgan Department of Radiology and Radiological Science, The Johns Hopkins
University School of Medicine, Baltimore, Maryland, USA.

⁸Shenzhen Research Institute, City University of Hong Kong, Shenzhen, China.

⁹Hong Kong Institutes of Medical Engineering, Hong Kong, China.

¹⁰Department of Electronic Engineering, Chinese University of Hong Kong, Hong Kong, China.

*Corresponding author(s). E-mail(s): yinidong@cityu.edu.hk;

Contributing authors: rrushuang2-c@my.cityu.edu.hk; zijunliu4-c@my.cityu.edu.hk;
lei.clifton@ndph.ox.ac.uk; david.clifton@eng.ox.ac.uk; KannieW.Y.C@cityu.edu.hk;
ytzhang@cuhk.edu.hk;

Abstract

Label scarcity problem is the main challenge that hinders the wide application of deep learning systems in automatic cardiovascular diseases (CVDs) detection using electrocardiography (ECG). Tuning pre-trained models alleviates this problem by transferring knowledge learned from large datasets to downstream small datasets. However, bottlenecks in computational efficiency and CVDs detection performance limit its clinical applications. It is difficult to improve the detection performance without significantly sacrificing model computational efficiency. Here, we propose a computation-efficient semi-supervised learning paradigm (FastECG) for robust and computation-efficient CVDs detection using ECG. It enables a robust adaptation of pre-trained models on downstream datasets with limited supervision and high computational efficiency. First, a random-deactivation technique is developed to achieve robust and fast low-rank adaptation of pre-trained weights. Subsequently, we propose a one-shot rank allocation module to determine the optimal ranks for the update matrices of the pre-trained weights. Finally, a lightweight semi-supervised learning pipeline is introduced to enhance model performance by leveraging labeled and unlabeled data with high computational efficiency. Extensive experiments on four downstream ECG datasets demonstrate that FastECG not only outperforms the state-of-the-art methods in multi-label CVDs detection but also consumes fewer GPU footprints, training time, and parameter storage space. As such, this paradigm provides an effective solution for achieving high computational efficiency and robust detection performance in the clinical applications of pre-trained models under limited supervision.

Keywords: Electrocardiograph, Pre-trained models, Semi-supervised learning, Computation-efficient, Cardiovascular diseases.

1 Introduction

Cardiovascular diseases have become the deadliest 'killer' of human health in recent years[1]. As a non-invasive and low-cost tool, ECG provides a visual representation of the electrical activity of the heart and is widely used in the detection of various CVDs[2, 3]. Benefiting from recent progress in computing hardware, ECG-based deep learning systems have achieved notable success in automatic CVDs detection[4–6]. However, previous deep learning models required sufficient labeled samples to achieve satisfactory performance when trained on new application scenarios with unseen CVDs[7, 8]. However, collecting well-labeled ECG recordings requires physicians' expertise and their laborious manual annotation, and therefore is expensive and time consuming in clinical practice[9, 10]. Additionally, constantly updating models to adapt to different downstream datasets often introduces heavy computational burdens[11]. As such, designing a fast and robust deep learning paradigm for ECG-based CVDs detection under limited supervision is highly in demand but remains challenging.

Recent advancements in pre-trained models (PMs) have enhanced the performance of deep learning models on the downstream datasets without large-scale labeled data[12–14]. A commonly used pipeline consists of pre-training over-parameterized backbone models on large-scale datasets, and then fine-tuning them on small downstream datasets in a supervised manner. In this process, the prior knowledge learned from the large datasets during pre-training is transferred to the downstream datasets, thereby improving the model performance on new application scenarios[15]. For instance, Kiyasseh *et al.* proposed a self-supervised method to pre-train a large model for ECG-based CVDs detection[16]. Their fine-tuned model demonstrated robust performance on downstream datasets with only 25% of labeled data. Subsequently, using 8 million ECG recordings, Akhil *et al.* pre-trained a vision-transformer model with self-supervised masked image modeling to improve the fine-tuning performance on downstream datasets[17].

However, two bottlenecks still greatly limit the clinical application of CVDs detection systems based on PMs. **(1) The bottleneck in CVDs detection performance.** Fine-tuning of pre-trained models is currently conducted in a purely supervised manner. When the sample size of the labeled data is very scarce in the downstream datasets, model performance may drop due to over-fitting[18]. Fortunately, a large number of unlabeled data in the medical domain are relatively easy to collect. Semi-supervised learning (SSL) is able to extract sufficient information from the unlabeled data and outperform the supervised models trained with the same amount of labeled data[8, 19–22]. For example, self-tuning integrates the exploration of unlabeled data and the knowledge transfer of PMs into a united framework, which significantly outperforms supervised fine-tuning on five downstream tasks[18]. Oliveira *et al.* conducts a comprehensive comparison analysis between SSL and supervised methods in ECG-based CVDs detection, demonstrating the superior performance of the SSL methods. Utilizing a knowledge distillation mechanism, MixTeacher delivers an effective SSL framework for atrial fibrillation detection under limited supervision, reducing the workload of ECG recordings annotation by 98%[9]. Despite their robust performance, existing SSL methods are mainly built on pseudo-label techniques and the weak-strong consistency training on unlabeled samples[7, 8, 21, 23, 24], which greatly increase the GPU memory footprint and computation time during model training. Furthermore, SSL methods using teacher-and-student models for knowledge distillation require two full copies of the corresponding PMs, thus increasing the model storage consumption. Therefore, it is necessary to address the bottleneck of computational efficiency during the performance enhancement of PMs using semi-supervised learning.

(2) The bottleneck in computational efficiency. Fine-tuning and SSL methods both update all the parameters of PMs. Despite their effectiveness, both methods have the main drawback that the tuned models have the same number of parameters as PMs, thus being computationally inefficient as the PMs scale up. Specifically, they require saving the gradients of all the parameters in PMs and even the momentum parameters, resulting in large GPU memory footprints when training large PMs[25]. Additionally, each tuned model can be regarded as a full copy of the corresponding PMs, and therefore leading to high storage consumption when simultaneously tuned on multiple datasets [26]. To address this, parameter-efficient fine-tuning (PEFT) methods have been introduced to reduce the trainable parameters during model training [11, 27, 28]. For example, BitFit[27] only tunes the bias terms in pre-trained models while freezing the remaining parameters, greatly reducing the number of trainable parameters. Low-rank adaptation (LoRA) achieves the same goal by updating the pre-trained weights with low-rank decomposition matrices. Consequently, parameter-efficient methods provide an effective solution to achieve parameter-efficient semi-supervised learning by integrating with different SSL methods. Despite their parameter efficiency, a comprehensive study concluded that they could not achieve on-par performance with fine-tuning on some complex downstream tasks[29]. AdaLoRA and IncreLoRA further improve the performance of LoRA by allocating different ranks to different pre-trained weights based on their importance[26, 30]. However, the above performance improvement is achieved at the cost of increased training time for iterative importance estimation.

Therefore, a dilemma is encountered: model performance improvement often comes at the expense of a large sacrifice of computational efficiency. Specifically, semi-supervised learning enhances CVDs detection performance, but at a significantly increased computational cost. Conversely, parameter-efficient methods that prioritize computational efficiency may compromise CVDs detection performance. Consequently, achieving a superior detection performance with high computation efficiency poses a great challenge to the clinical application of PMs in ECG-based CVDs detection.

In this study, we propose a united paradigm capable of addressing the above two bottlenecks simultaneously. It is a computation-efficient semi-supervised learning paradigm (FastECG) for adapting pre-trained models on downstream datasets with high computational efficiency under limited supervision. Our method enables robust and low-cost detection of CVDs in clinical practice using ECG recordings. As shown in Fig.1, first, a base backbone is pre-trained on a large-scale 12-lead ECG dataset in a supervised manner, which provides a foundation model for downstream tasks. Second, a random-deactivation low-rank adaptation (RD-LoRA) method formulates a low-cost and robust pipeline for updating the pre-trained backbone on downstream datasets. Specifically, it stochastically activates or deactivates low-rank adaptation in each trainable layer of the backbone with a probability p . To reduce GPU memory footprint, the pre-trained weights in each layer are always frozen. Theoretical analysis indicates that the random deactivation operation integrates various sub-networks generated during model training, thus overcoming the performance bottleneck in tuning PMs. Additionally, deactivating low-rank adaptation in some layers reduces computation costs and speeds up the training process, especially when the backbone model size is large. Third, a one-shot rank allocation module allocates the optimal ranks for the low-rank matrices in each layer. In contrast to AdaLoRA[26] and IncreLoRA[30], the proposed method is able to determine the optimal ranks using only one gradient backward iteration, improving the adaptation performance at low computational costs.

Additionally, a lightweight semi-supervised learning module is developed to leverage the abundant information within unlabeled data. This module uses unlabeled data to stabilize the statistics estimation in batch normalization layers, enhancing their generalization performance on unseen data distributions. Compared to the pseudo-labeling and the weak-strong consistency training methods[8, 23, 24], our lightweight module overcomes the label scarcity problem with significantly higher computational efficiency.

Finally, extensive experiments on four downstream ECG datasets demonstrate the superior CVDs detection performance of the proposed FastECG against various state-of-the-art models under very limited supervision. Most importantly, our method only requires 66.5% training time, 70.7% GPU memory footprint, and 1.8%-5.8% trainable parameters of the state-of-the-art SSL methods. In conclusion, our proposed computation-efficient semi-supervised learning paradigm provides an effective solution to overcome the two bottlenecks that limit the clinical applications of PMs in ECG-based CVDs detection.

2 Results

Designing a robust and low-cost deep learning paradigm for CVDs detection under label-scarcity conditions remains a challenge in medical intelligence. The proposed FastECG addresses this challenge by introducing a novel computation-efficient semi-supervised learning paradigm (Fig.1), which integrates four important sub-modules. We conduct extensive and systematic experiments to evaluate its effectiveness and computational efficiency on various public databases. Our results indicate that FastECG not only outperforms state-of-the-art semi-supervised and parameter-efficient semi-supervised baselines in ECG-based CVD detection but also demonstrates satisfactory computational efficiency.

2.1 Datasets and experiment protocols

In this section, we utilized a large-scale dataset to pre-train the backbone model and evaluated the performance of our FastECG on four downstream datasets. First, an openly available ECG dataset (CODE-15%) collected by the Telehealth Center of the Universidade Federal de Minas Gerais[5, 31] is used for base backbone pre-training. The CODE-15% dataset contains 15% of the ECG data from the restricted CODE-full dataset[5, 32]. Specifically, there are 345779 ECG recordings from 233770 patients in the CODE-15% dataset, alongside six CVD labels: 1st degree AV block (1dAVb), left bundle branch block (LBBB), right bundle branch block (RBBB), sinus tachycardia (ST), atrial fibrillation (AF) and sinus bradycardia (SB). Each ECG recording lasts 7-10s, and the sampling rate is 300-600 Hz. Subsequently, we use four small datasets for downstream model retraining and evaluation: the Georgia 12-lead ECG Challenge (G12EC) database[33], the Chapman-Shaoxing database[34], the Ningbo database[35], and the Physikalisch-Technische Bundesanstalt (PTB-XL) database[36]. Specifically, the G12EC database contains 10344 ECG recordings from 10,344 people, and the PTB-XL database comprises 21837 recordings from 18885 patients. The Chapman database contains 10,646 recordings from 10646 patients, and the Ningbo database encompasses 40258 recordings from 40258 patients. Only 34,905 recordings in the Ningbo database are publicly available[33].

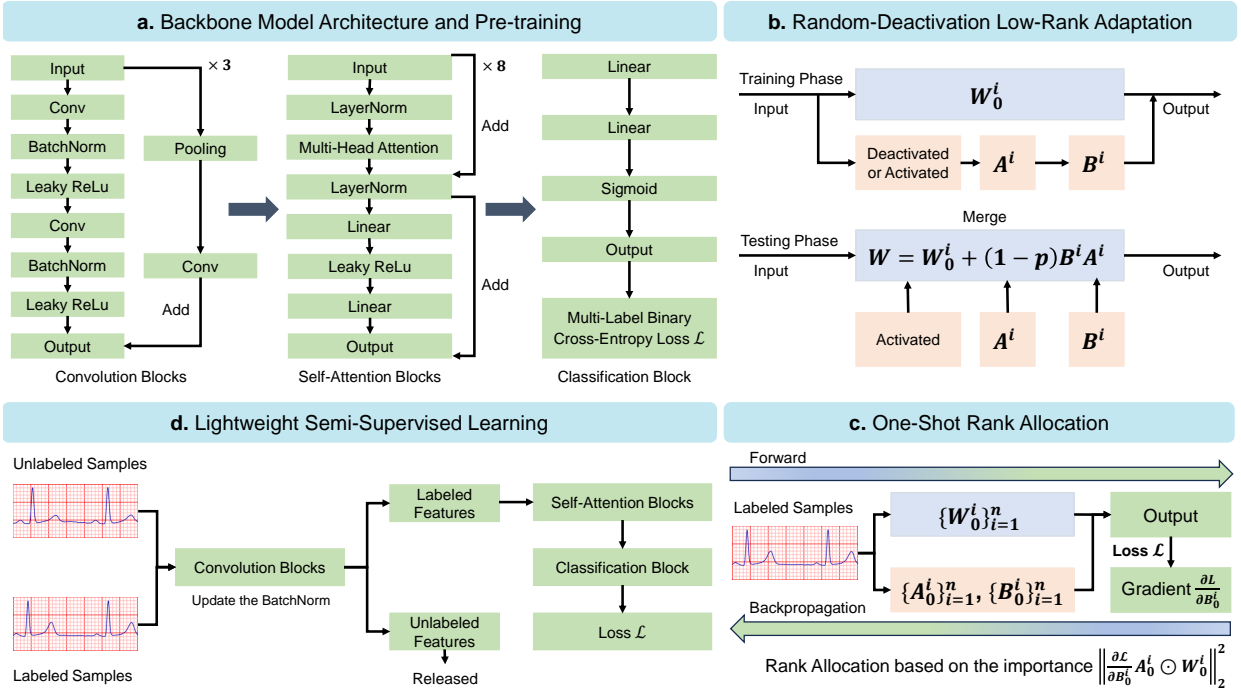


Fig. 1: Overview of FastECG. **a.** The architecture of the pre-trained backbone model. It consists of three convolution blocks, eight self-attention blocks, and one classification block in the base backbone. It is pre-trained on a public 12-lead ECG dataset using the supervised multi-label binary cross-entropy loss. **b.** **Random-deactivation low-rank adaptation.** On the downstream datasets, the pre-trained weights $\{W_0^i\}_{i=1}^n$ in the backbone are updated by the proposed random-deactivation low-rank adaptation. It randomly activates or deactivates the low-rank matrices ($\{B^i\}_{i=1}^n$ and $\{A^i\}_{i=1}^n$) in each trainable layer with a given probability p . Note that all the pre-trained weights are frozen during model training. All the low-rank matrices are activated and merged into the pre-trained weights in the testing stage. The merge process generates an ensemble network combining all the sub-networks produced by the random deactivation operation. **c.** **One-shot rank allocation.** The ranks of the low-rank matrices are determined by the proposed one-shot rank allocation method using only one gradient backward on the labeled samples. The matrices with high importance are allocated with a higher rank than those with low importance. **d.** **Lightweight semi-supervised learning.** During the low-rank adaptation process, unlabeled samples from the downstream datasets are combined with the labeled samples to estimate the statistics in batch-normalization layers. Subsequently, only the labeled data is forwarded to the self-attention blocks for CVDs detection, and the unlabeled data is released in GPU memory. This lightweight semi-supervised pipeline improves the model performance in a computational-efficient way.

The recordings from the four downstream databases are around 10 seconds, and the sampling rate is 500 Hz. Additionally, each database contains over 17 different CVDs, and multiple CVDs can be identified from one ECG segment simultaneously.

The base backbone model is first pre-trained on the CODE-15% dataset using the ECG recordings and the corresponding multi-label ground truths. The architecture of the backbone is shown in Fig.1. AdawW optimizer[37] is used for the pre-training process with a learning rate of 1e-3 and a batch size of 1024. Then, the pre-trained backbone is retrained on the four downstream datasets using different methods under limited supervision. Taking the G12EC database as an example, the ECG recordings are split into a training set and a held-out test set in a ratio of 0.9: 0.1. Then, the training set is divided into a labeled training set and an unlabeled training set in a ratio of 0.05: 0.95. A validation set is randomly sampled from the labeled training set and accounts for 20% of it, which is used for selecting the best-performing model during training. For model comparisons, we reproduce several baseline models in semi-supervised learning: ReMixMatch[23], FixMatch[8], FlexMatch[21], SoftMatch[24], MixedTeacher[9], Adsh[38], SAW[39], and parameter-efficient methods: LoRA[25], DyLoRA[40], AdaLoRA[26], IncreLoRA[30].

We comprehensively evaluate the model performance of various methods using multiple metrics and training costs. Since multiple CVDs can be detected from one recording simultaneously, we used metrics on multi-label classification. Our metrics include ranking loss, coverage, mean average precision (MAP), macro AUC, macro $G_{\beta=2}$, and macro $F_{\beta=2}$. We set the β value to be 2 for all the corresponding experiments following the configurations provided in ref.[41]. Lower values indicate better model performance in the first

two metrics (ranking loss and coverage), whereas the inverse holds for the remaining metrics. A detailed computation process for the metrics can be found in Supplementary Materials Section 1. Additionally, we report the training costs of different models. Specifically, the GPU memory footprint (Mem), the number of trainable parameters (Params), and the averaged training time for each optimization iteration (Time/iter) are presented. The higher the number of trainable parameters, the higher the parameter storage consumption. Note that the number of trainable parameters of FastECG can be adjusted by the initial rank r . Lower ranks indicate fewer trainable parameters. The AdamW optimizer[37] is used under a learning rate of 1e-3 and a batch size of 64 for all the compared methods. All the experiments are conducted in a single NVIDIA A6000 graphics processing unit using the Pytorch library.

2.2 Analysis of the cardiovascular diseases detection result

Table 1 shows that our proposed FastECG achieved superior detection performance on four datasets with the lowest computational costs compared with the baseline models. For example, in the G12EC dataset, FastECG with $r = 16$ achieves a macro $F_{\beta=2}$ of 0.551 ± 0.017 , which is 4.1% larger than the second-best model’s (FixMatch) performance. In Supplementary Materials Section 2, we present the detection performance of different models on each CVD. The results demonstrate that FastECG ranks the best in some CVDs, such as atrial fibrillation and first-degree AV block. It also achieves comparable performance to the compared methods in the remaining CVDs. Regarding computational costs, it requires 33.5% less training time than MixedTeacher, occupies 29.3% less GPU memory than Adsh, and has only 5.8% of the trainable parameters found in them. When the initial rank r decreases to 4, FastECG shows a slight performance drop in four datasets, but the number of trainable parameters further decreases to 1.8% of the baseline models. This observation indicates the stability and robustness of the FastECG under extremely low parameter budgets.

We further compare the proposed FastECG with the parameter-efficient methods, which are integrated with FixMatch for parameter-efficient semi-supervised learning. For example, FixMatch with low-rank adaptation (LoRA) is denoted as ‘FixMatch+LoRA’. Similar to the FastECG, their budgets for the number of trainable parameters are controlled by the initial rank r . As illustrated in Fig. 2, we report their macro- $F_{\beta=2}$ scores, macro- $G_{\beta=2}$ scores, and Time/iter on four datasets at sufficient ($r = 16$) and limited ($r = 4$) budget levels. The macro- $F_{\beta=2}$ and macro- $G_{\beta=2}$ scores of the FixMatch without parameter-efficient training (Params: 9.505M) are denoted as gray dotted lines. The experiment results indicate that FastECG consistently outperforms the other methods on four datasets at different budget levels. Under a sufficient parameter budget ($r = 16$), FastECG achieves a macro- $G_{\beta=2}$ score of 0.307 ± 0.016 on the G12EC dataset, which is 2.8% higher than the FixMatch with LoRA. When the parameter budget is limited ($r = 4$), FastECG still outperforms it by 1.5%. Additionally, FastECG achieves the highest training speed and the best performance with the least trainable parameters compared to other parameter-efficient semi-supervised learning frameworks. On the four datasets, FastECG requires 50% less training time compared to other methods. This phenomenon demonstrates the computational efficiency of the proposed FastECG. The Extended Data Table 1 presents detailed comparison results on more evaluation metrics, which provides supplementary evidence on the efficiency of the proposed FastECG in CVDs detection. Paired t-tests are conducted to evaluate the significance levels of the performance difference between FastECG and the aforementioned SOTA methods (Supplementary Materials Section 3 Fig. S1). Based on the calculated two-sided p -value, it can be observed that FastECG outperforms the baselines at a 0.05 significance level in most datasets and evaluation metrics, which indicates a significant superiority for the proposed FastECG framework.

In summary, our experiment results demonstrate the robustness and computational efficiency of the FastECG in semi-supervised cardiovascular disease detection at different parameter budget levels. In other words, FastECG can enhance the detection performance of ECG-based CVDs detection models without introducing heavy computation burdens.

2.3 Effect of the ratio of labeled samples

Here, we compare the proposed FastECG and baseline models under various ratios of labeled samples in the datasets. Specifically, we adjust the ratio of the labeled samples in the dataset from 5% to 15% and present the averaged performance of different models on the four datasets in Fig. 3a. The experiment results demonstrate the superiority of the proposed FastECG compared with FixMatch and FixMatch with LoRA under various ratios of the labeled data, especially when the ratio is low. As the ratio decreases from 15% to 5%, the performance advantage of FastECG over other models becomes more significant. When using 15% labeled data, FastECG achieves improvements of 1.3% on the macro $F_{\beta=2}$ compared to FixMatch with LoRA. In contrast, FastECG outperforms it by 1.9% on the macro $F_{\beta=2}$ using 5% labeled data. In

Table 1: Performance comparisons of FastECG and semi-supervised baselines on the base backbone. The average performance on all CVDs within each dataset is shown across six seeds. The standard deviation is also reported for the evaluation metrics.

Methods	Params ↓	Mem ↓	Time/iter ↓	Ranking Loss ↓	Coverage ↓	Macro AUC ↑	MAP ↑	Macro $G_{\beta=2}$ ↑	Macro $F_{\beta=2}$ ↑
G12EC Dataset									
ReMixMatch	9.505 M	7.699 GB	271 ms	0.178±0.033	5.635±0.529	0.759±0.015	0.310±0.019	0.184±0.017	0.387±0.031
MixedTeacher	9.505 M	3.941 GB	147 ms	0.107±0.009	4.224±0.236	0.835±0.010	0.464±0.003	0.275±0.016	0.507±0.025
FixMatch	9.505 M	5.784 GB	187 ms	0.107±0.006	4.292±0.163	0.829±0.004	0.468±0.009	0.280±0.010	0.510±0.016
FlexMatch	9.505 M	5.784 GB	187 ms	0.113±0.005	4.365±0.133	0.829±0.009	0.450±0.022	0.274±0.019	0.497±0.035
SoftMatch	9.505 M	5.784 GB	187 ms	0.110±0.006	4.313±0.128	0.834±0.004	0.457±0.010	0.276±0.017	0.504±0.021
Adsh	9.505 M	3.887 GB	207 ms	0.111±0.003	4.387±0.129	0.827±0.005	0.458±0.007	0.268±0.009	0.489±0.013
SAW	9.505 M	5.784 GB	188 ms	0.112±0.003	4.369±0.105	0.827±0.005	0.459±0.017	0.269±0.018	0.494±0.024
FastECG_{r=16}	0.510 M	2.747 GB	98 ms	0.092±0.002	3.867±0.088	0.855±0.005	0.476±0.006	0.307±0.016	0.551±0.017
FastECG_{r=4}	0.183 M	2.743 GB	98 ms	0.089±0.003	3.804±0.095	0.853±0.004	0.467±0.006	0.304±0.013	0.553±0.020
PTB-XL Dataset									
ReMixMatch	9.505 M	7.699 GB	301 ms	0.068±0.008	3.699±0.196	0.827±0.006	0.350±0.010	0.212±0.015	0.423±0.028
MixedTeacher	9.505 M	3.941 GB	164 ms	0.037±0.003	2.841±0.095	0.884±0.008	0.509±0.008	0.316±0.007	0.542±0.014
FixMatch	9.505 M	5.784 GB	208 ms	0.038±0.001	2.905±0.061	0.882±0.004	0.510±0.006	0.322±0.007	0.541±0.007
FlexMatch	9.505 M	5.784 GB	209 ms	0.039±0.001	2.937±0.048	0.887±0.005	0.505±0.005	0.316±0.008	0.536±0.007
SoftMatch	9.505 M	5.784 GB	209 ms	0.039±0.003	2.919±0.097	0.885±0.006	0.508±0.007	0.317±0.009	0.540±0.011
Adsh	9.505 M	3.887 GB	316 ms	0.038±0.002	2.879±0.054	0.886±0.004	0.511±0.005	0.322±0.008	0.543±0.015
SAW	9.505 M	5.784 GB	208 ms	0.037±0.003	2.855±0.093	0.889±0.005	0.520±0.007	0.323±0.019	0.548±0.017
FastECG_{r=16}	0.582 M	2.748 GB	110 ms	0.031±0.000	2.641±0.020	0.901±0.003	0.530±0.005	0.346±0.006	0.578±0.006
FastECG_{r=4}	0.159 M	2.744 GB	109 ms	0.030±0.001	2.626±0.026	0.899±0.004	0.526±0.005	0.346±0.005	0.580±0.006
Ningbo Dataset									
ReMixMatch	9.506 M	7.699 GB	312 ms	0.071±0.010	3.999±0.231	0.867±0.008	0.338±0.024	0.214±0.016	0.430±0.020
MixedTeacher	9.506 M	3.941 GB	173 ms	0.035±0.002	2.982±0.077	0.925±0.006	0.496±0.020	0.324±0.018	0.549±0.028
FixMatch	9.506 M	5.784 GB	217 ms	0.035±0.003	3.025±0.121	0.922±0.009	0.493±0.023	0.321±0.014	0.545±0.020
FlexMatch	9.506 M	5.784 GB	217 ms	0.037±0.002	3.078±0.090	0.921±0.007	0.489±0.024	0.318±0.012	0.544±0.019
SoftMatch	9.506 M	5.784 GB	217 ms	0.035±0.001	3.018±0.049	0.923±0.005	0.496±0.024	0.321±0.014	0.552±0.020
Adsh	9.506 M	3.887 GB	423 ms	0.035±0.002	3.007±0.090	0.921±0.004	0.492±0.023	0.318±0.010	0.545±0.012
SAW	9.506 M	5.784 GB	215 ms	0.037±0.001	3.064±0.036	0.924±0.004	0.492±0.024	0.314±0.010	0.536±0.016
FastECG_{r=16}	0.550 M	2.748 GB	115 ms	0.030±0.001	2.805±0.063	0.928±0.002	0.505±0.019	0.334±0.011	0.569±0.014
FastECG_{r=4}	0.168 M	2.744 GB	114 ms	0.030±0.001	2.776±0.028	0.929±0.001	0.500±0.017	0.327±0.010	0.567±0.011
Chapman Dataset									
ReMixMatch	9.504 M	7.699 GB	270 ms	0.101±0.025	3.574±0.393	0.839±0.011	0.403±0.015	0.246±0.018	0.428±0.020
MixedTeacher	9.504 M	3.941 GB	148 ms	0.047±0.002	2.615±0.068	0.889±0.012	0.519±0.018	0.327±0.019	0.510±0.024
FixMatch	9.504 M	5.784 GB	186 ms	0.046±0.004	2.626±0.096	0.897±0.006	0.520±0.009	0.339±0.012	0.518±0.025
FlexMatch	9.504 M	5.784 GB	185 ms	0.047±0.004	2.659±0.103	0.895±0.006	0.518±0.008	0.325±0.010	0.495±0.019
SoftMatch	9.504 M	5.784 GB	187 ms	0.047±0.004	2.649±0.079	0.898±0.006	0.525±0.012	0.335±0.011	0.511±0.021
Adsh	9.504 M	3.887 GB	207 ms	0.046±0.004	2.621±0.117	0.896±0.005	0.528±0.008	0.335±0.013	0.517±0.020
SAW	9.504 M	5.784 GB	185 ms	0.049±0.003	2.699±0.072	0.897±0.007	0.524±0.009	0.333±0.012	0.510±0.020
FastECG_{r=16}	0.581 M	2.748 GB	97 ms	0.040±0.002	2.483±0.055	0.896±0.006	0.536±0.004	0.355±0.005	0.530±0.008
FastECG_{r=4}	0.180 M	2.743 GB	97 ms	0.038±0.002	2.418±0.049	0.898±0.005	0.526±0.006	0.352±0.009	0.530±0.012

Extend Data Fig.1, we also compare FastECG with other baseline models, where FastECG consistently outperforms them in CVDs detection under various labeled ratios.

2.4 Rank initialization in the one-shot rank allocation

Rank initialization is an important component in low-rank adaptation, which controls the number of trainable parameters during model training. In this section, we adjust the initial rank from 4 to 32 and present the averaged model performance on the four datasets in Fig.3b. Note that the labeled ratio is set to 5%. The results indicate that FastECG with high initial ranks ($r = 16, 32$) achieves better performance than that with low initial ranks ($r = 4, 8$). This is because the model with higher ranks has more trainable parameters and thus demonstrates a larger capacity during training.

2.5 Effect of the number of important weight matrices

Based on the proposed one-shot rank allocation, FastECG allocates a rank r to the incremental matrices with high importance and a rank $r/2$ to the matrices with low importance. The ratio of the important matrices to the total number of pre-trained matrices is defined as the coefficient c . The higher the coefficient is, the higher the ratio of the important matrices. In Fig.3c, we adjust the coefficient from 0.2 to 0.8 and

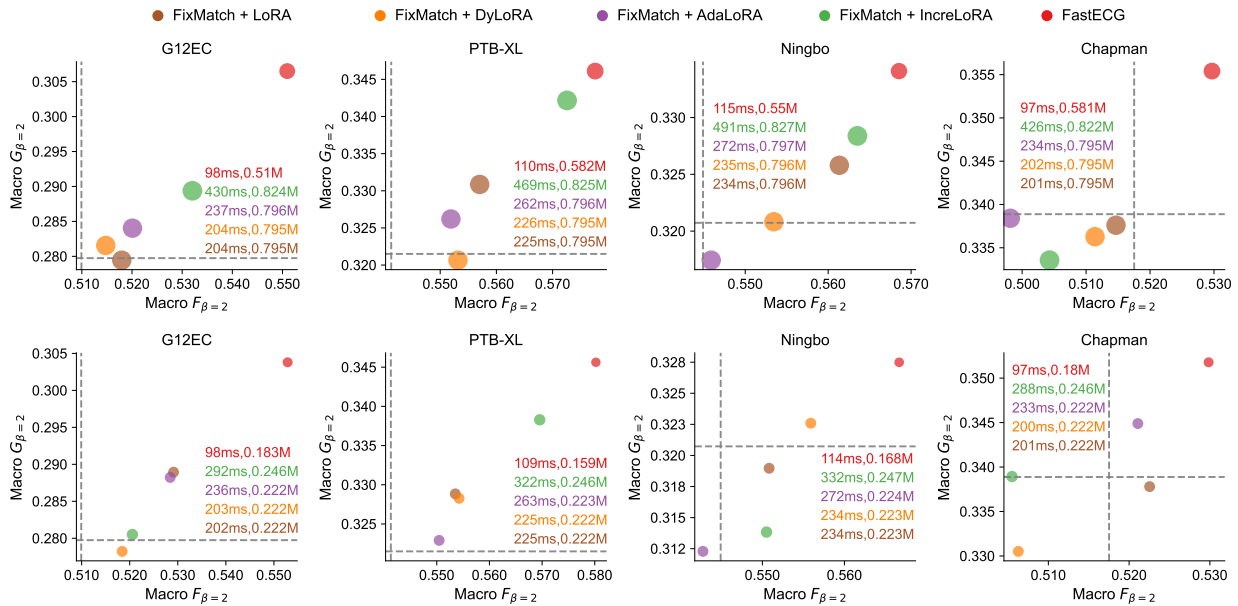


Fig. 2: Comparison between FastECG and parameter-efficient semi-supervised methods on the base backbone. Circles with various colors denote different models, and their size represents the number of trainable parameters. The training time for each optimization iteration (Time/iter) of different methods is also reported. The gray dotted lines represent the performance of the FixMatch baseline without parameter-efficient training (approximately 9.505M trainable parameters). The first row of the figure presents the performance of different models with sufficient parameter budgets ($r = 16$), while the second row reports their performance under limited parameter budgets ($r = 4$).

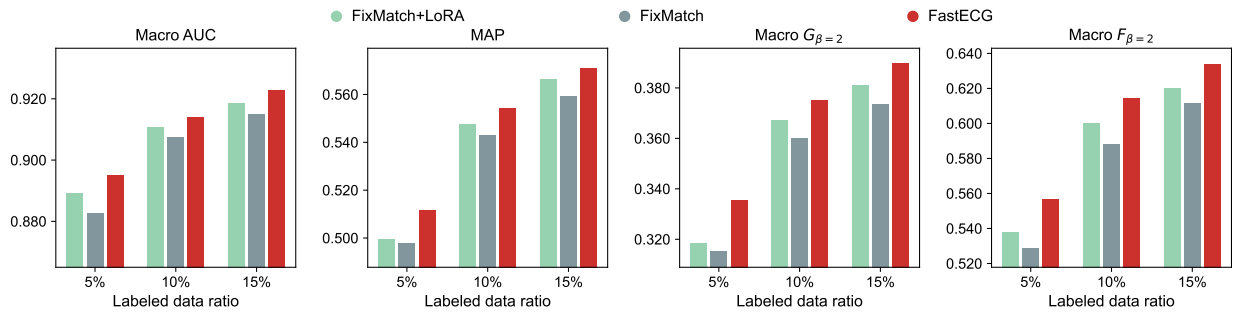
report the averaged model performance across four datasets. Note that the labeled ratio is set to 5%, and the initial ranks r for all the low-rank matrices are set to 16. It can be observed that the performance of the proposed model is relatively insensitive to the changes in the c . In the Extended Data Fig.2, we visualize the rank distribution generated by the proposed method under various coefficients c . When the ratio of important matrices decreases from 0.8 to 0.2, the proposed method allocates more ranks to the self-attention and classification blocks than the convolution blocks. This phenomenon indicates that the deep modules exhibit higher importance than the shallow modules during model training, which aligns with the conclusions made by previous studies[26, 42].

2.6 Effect of the deactivation probability

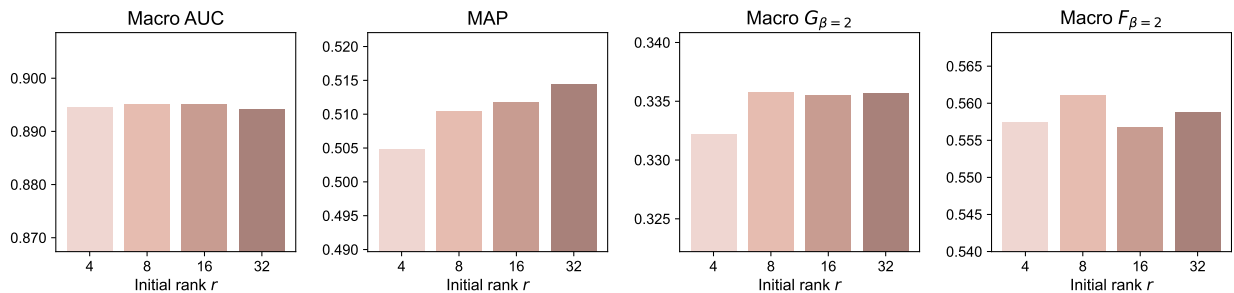
For each pre-trained weight W_0^i in the FastECG, the proposed RD-LoRA deactivates its low-rank matrices (A^i, B^i) in the current iteration at a probability of p , which produces multiple sub-networks during model training. All the low-rank matrices are activated in the testing stage, generating an ensemble network that combines all the sub-networks. Consequently, the probability p is an important parameter that controls the training time and the final performance of the proposed FastECG. In Fig.3d, we adjust p from 0.1 to 0.5 and present the averaged model performance across four datasets, including the training time for each iteration. Note that the labeled ratio is set to 5%, and the initial ranks for all the low-rank matrices are set to 16. The results show that the FastECG with $p = 0.2$ demonstrates the best detection performance compared with the model with other settings. In addition, it can be observed that the training time of the FastECG decreases as p increases. The reason is that the larger the p is, the more low-rank matrices are deactivated during model training, which speeds up the forward-backward propagation.

2.7 Performance comparisons under different backbone sizes

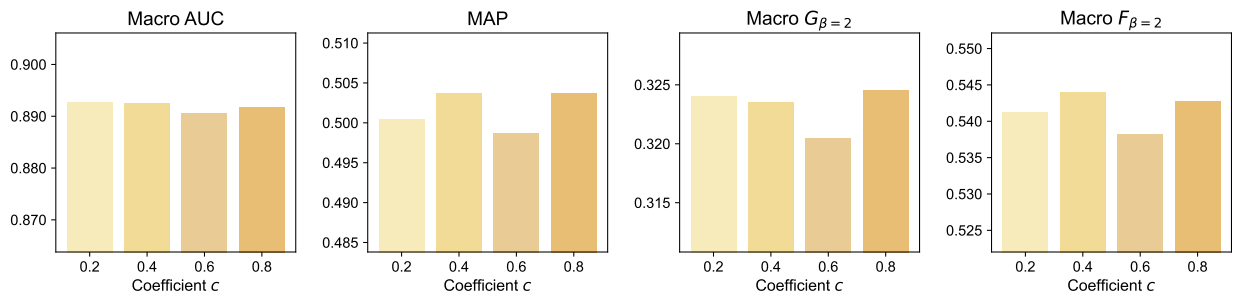
Previous studies have demonstrated that the backbones pre-trained on a large-scale dataset with a large model size usually have better performance than the other backbones[43, 44]. In the previous sections, we have already proved the robustness and computation efficiency of the proposed FastECG under a base backbone with 9.505 million parameters. Here, we compare its performance with other baseline models under medium and large backbones, which share the same architecture as the base backbone but have more parameters. Specifically, the medium backbone has 50.494 million parameters, and the large backbone has 113.490 million parameters (Extended Data Table 2). They are pre-trained on the CODE-full dataset, a huge but restricted ECG dataset with 2,322,513 ECG recordings from 1,558,772 patients[5, 31]. In Extended Data



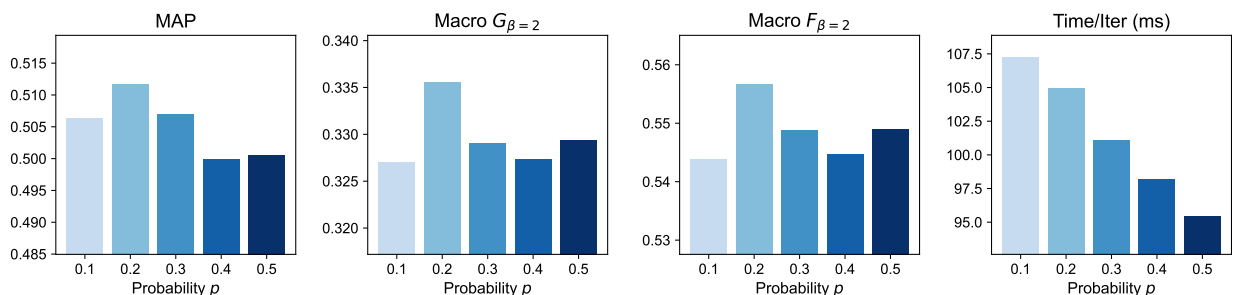
(a) Effect of the ratio of labeled samples for model training



(b) Effect of the rank initialization



(c) Effect of the ratio of important weight matrices



(d) Effect of the deactivation probability

Fig. 3: The sensitivity analysis on the FastECG with the base backbone. (a) We adjust the ratio of the labeled samples in the dataset from 0.05 to 0.15 and report the averaged performance of different models across four datasets and six random seeds. (b) Averaged performance of the FastECG across four datasets and six random seeds under different initial ranks r . (c) We adjust the ratio of the important weight matrices to the total number of weight matrices and report the averaged performance across four datasets and six random seeds. Important weights are adapted with rank r while the remaining weights are adapted with rank $\frac{1}{2}r$. (d) Averaged performance and training time of the FastECG across four datasets and six random seeds under different deactivation probability p .

Table 3 and Table 4, we report the performance of FastECG and semi-supervised baselines on the medium and the large backbones, respectively. The results demonstrate that FastECG achieves similar and even better CVDs detection performance than the semi-supervised baselines and exhibits the lowest computation costs. For example, using the medium backbone, FastECG achieves a macro $F_{\beta=2}$ of 0.599 ± 0.010 , which is 3.7% larger than the second-best model’s (SAW) performance in the PTB-XL dataset. Using the large backbone, FastECG achieves a macro $F_{\beta=2}$ of 0.565 ± 0.010 in the G12EC dataset, outperforming SAW by 3.1%. Regarding the computational costs, the number of trainable parameters of FastECG is 0.9% to 3.1% of the other baselines on the medium backbone and 0.6% to 2.1% on the large backbone. In addition, FastECG demonstrates the lowest GPU memory consumption and the highest training speed compared to the other semi-supervised baselines. For the memory footprint, FastECG achieves an average GPU memory usage of 6.16 GB using the medium backbone and 9.22 GB using the large backbone, 3.09 GB and 4.59 GB less than the second-best model (Adsh). Furthermore, FastECG achieves an average training time per iteration of 259.25 ms using the medium backbone and 485.5 ms using the large backbone, 162.5 ms and 289.75 ms faster than the second-best model (MixedTeacher). These phenomena demonstrate that as the number of model parameters increases, the computational efficiency advantage of FastECG over other models becomes increasingly apparent. In Extended Data Table 5 and Table 6, we present the performance of FastECG and parameter-efficient semi-supervised methods on the medium and large backbones, respectively. It can be observed that FastECG outperforms the other models in CVDs detection on both medium and large backbones. Additionally, FastECG demonstrates the fastest training speed across four datasets compared with other parameter-efficient methods. In Supplementary Materials Section 3 Fig. S2-S3, we provide the paired t-test results of the model performance on the two backbones. The statistical results indicate that FastECG outperforms the above baselines in ECG-based CVDs detection at a 0.05 significance level in most conditions.

2.8 Ablation study

We conducted an ablation study to evaluate the contribution of the modules implemented in FastECG. Specifically, we remove each of the proposed three modules from the FastECG and record the corresponding model performance on the four datasets. Note that the initial rank r is 16 for all the compared models.

(1) The random-deactivation low-rank adaptation improves model performance and computational efficiency. It randomly deactivates the low-rank matrices in each trainable layer with a given probability, which generates multiple sub-networks during model training. All the low-rank matrices are activated in the testing stage, and the sub-networks are merged into a robust ensemble network. In the G12EC dataset, the FastECG with the random deactivation module increases the macro $F_{\beta=2}$ from 0.536 ± 0.021 to 0.551 ± 0.017 and decreases the ranking loss from 0.095 ± 0.004 to 0.092 ± 0.002 . Additionally, the Time/iter is reduced from 104 ms to 98 ms. This observation indicates that the computation cost of training a sub-network with fewer low-rank matrices is lower than optimizing the entire network. **(2) The one-shot rank allocation method improves low-rank adaptation performance with high computational efficiency.** One drawback of LoRA[25] is its inability to allocate an optimal rank for each incremental matrix[26, 30]. Here, the proposed rank allocation method determines the optimal ranks using only one gradient-backward iteration with high computational efficiency. As shown in Table 2, removing the proposed module decreases the detection performance of FastECG in the four datasets. For example, the macro $F_{\beta=2}$ decreases from 0.530 ± 0.008 to 0.514 ± 0.018 and the coverage increases from 2.483 ± 0.055 to 2.503 ± 0.040 on the Chapman dataset. Additionally, it can be observed that the one-shot rank allocation module does not introduce heavy computational burdens (Time/iter only increases by 1-2ms), demonstrating its high computational efficiency. **(3) The proposed lightweight semi-supervised learning benefits model performance under limited supervision without greatly increasing the training time.** It utilizes the unlabeled data to stabilize the statistics within the BN layers in the convolution blocks, preventing them from over-fitting to small amounts of labeled data. When the module is removed, the performance of the FastECG decreases on all the datasets. For example, the macro $F_{\beta=2}$ score decreases from 0.551 ± 0.017 to 0.536 ± 0.029 on the G12EC dataset. Compared to other semi-supervised baselines (Table 1), the extra computation costs (Time/iter only increases by 20ms) caused by the proposed module are much lower. In Supplementary Materials Section 3, ablation studies on the medium and large backbones are provided, consistently demonstrating the notable contribution of the proposed three techniques.

3 Discussion

Bottlenecks in model performance and computational efficiency have become great challenges in the clinical application of CVDs detection systems based on pre-trained models, especially when the supervised information is scarce in the downstream ECG datasets. Previous studies usually overcome the performance bottleneck at the cost of a large drop in computational efficiency[18, 22, 26, 30]. In this paper, we propose

Table 2: Ablation study of the proposed FastECG on the base backbone. 'w/o random deactivation' represents the FastECG without the random deactivation technique, and the deactivation probability p is set to zero. 'w/o rank allocation' represents the FastECG without the one-shot rank allocation, and all pre-trained weights are updated with the initial rank $r = 16$. 'w/o unlabeled data' denotes the FastECG without the unlabeled data for lightweight semi-supervised learning.

Methods	Time/iter ↓	Ranking Loss ↓	Coverage ↓	Macro AUC ↑	MAP ↑	Macro $G_{\beta=2}$ ↑	Macro F_{beta} ↑
G12EC Dataset							
w/o random deactivation	104ms	0.095±0.004	3.954±0.163	0.848±0.007	0.470±0.007	0.294±0.015	0.536±0.021
w/o rank allocation	97ms	0.092±0.002	3.848±0.049	0.849±0.007	0.467±0.009	0.294±0.016	0.537±0.019
w/o unlabeled data	78ms	0.092±0.002	3.895±0.104	0.854±0.004	0.475±0.011	0.297±0.021	0.536±0.029
FastECG	98ms	0.092±0.002	3.867±0.088	0.855±0.005	0.476±0.006	0.307±0.016	0.551±0.017
PTB-XL Dataset							
w/o random deactivation	115ms	0.034±0.002	2.741±0.062	0.890±0.005	0.516±0.009	0.328±0.012	0.554±0.011
w/o rank allocation	108ms	0.032±0.001	2.692±0.046	0.895±0.003	0.530±0.005	0.332±0.011	0.560±0.014
w/o unlabeled data	87ms	0.031±0.002	2.670±0.064	0.899±0.004	0.532±0.006	0.332±0.010	0.565±0.007
FastECG	110ms	0.031±0.000	2.641±0.020	0.901±0.003	0.530±0.005	0.346±0.006	0.578±0.006
Ningbo Dataset							
w/o random deactivation	121ms	0.032±0.003	2.887±0.085	0.925±0.005	0.497±0.015	0.321±0.013	0.553±0.017
w/o rank allocation	114ms	0.030±0.001	2.801±0.023	0.928±0.002	0.497±0.021	0.325±0.010	0.563±0.014
w/o unlabeled data	92ms	0.031±0.001	2.821±0.058	0.929±0.003	0.499±0.017	0.325±0.012	0.559±0.018
FastECG	115ms	0.030±0.001	2.805±0.063	0.928±0.002	0.505±0.019	0.334±0.011	0.569±0.014
Chapman Dataset							
w/o random deactivation	102ms	0.041±0.003	2.505±0.080	0.895±0.010	0.526±0.005	0.335±0.012	0.514±0.015
w/o rank allocation	96ms	0.041±0.001	2.503±0.040	0.892±0.008	0.527±0.012	0.346±0.007	0.514±0.018
w/o unlabeled data	77ms	0.040±0.002	2.468±0.050	0.896±0.010	0.533±0.010	0.350±0.020	0.527±0.026
FastECG	97ms	0.040±0.002	2.483±0.055	0.896±0.006	0.536±0.004	0.355±0.005	0.530±0.008

a computationally efficient semi-supervised learning paradigm (FastECG) for adapting the PMs on downstream datasets with limited supervision and high computational efficiency. Experiment results on four downstream ECG datasets and three backbone settings indicate that FastECG achieves superior CVDs detection performance and computational efficiency compared to state-of-the-art methods.

Our proposed FastECG paradigm enhances the performance of pre-trained models without a large sacrifice of computational efficiency, including GPU memory footprint, training time, and storage consumption. Through integrating the sub-networks generated by the random-deactivation operation, the expected CVDs detection performance of FastECG is superior to the other compared methods, such as LoRA[25] and DyLoRA[40]. Its training time is also decreased due to omitting the computation of the update matrices for the deactivated low-rank matrices. In addition, determining the optimal rank distribution is a popular method to improve the low-rank adaptation performance of the pre-trained models. However, AdaLoRA[26] and IncreLoRA[30] continuously adjust the optimal ranks during the training process, decreasing the model computation efficiency. In contrast, the one-shot allocation method avoids this by determining the optimal ranks using only one forward-backward propagation before model training. In the downstream ECG datasets, the label scarcity problem is a crucial factor that results in the performance bottleneck of pre-trained models. Although semi-supervised learning offers an effective solution to address the label scarcity problem and overcome the bottleneck[21, 24, 45, 46], the commonly utilized semi-supervised techniques such as consistency training can be expensive in large pre-trained models and greatly increase their training time[47]. In contrast, FastECG adopts a lightweight semi-supervised learning pipeline, which leverages the unlabeled data to stabilize the statistic estimation in batch normalization layers. The extracted features of unlabeled data can be released in the self-attention blocks, which saves a lot of GPU memory footprint and computation time. Our results demonstrate that the lightweight semi-supervised learning method can help FastECG overcome the performance bottleneck without significantly decreasing its computational efficiency. In summary, the theoretical and empirical analysis indicates that FastECG is able to improve the detection performance and computational efficiency simultaneously.

In conclusion, our study offers a fast and robust semi-supervised learning paradigm for ECG-based CVDs detection under limited supervision. It provides a feasible solution for efficiently adapting pre-trained models on downstream ECG datasets. We hope this learning paradigm will pave the way for the application of automatic CVDs detection systems and broaden its applicability to various ECG-based tasks.

Our FastECG has a limitation that should be addressed before its clinical application. The class-imbalance problem limits the model performance on ECG recordings with rare CVDs. It tends to make negative predictions on the rare CVDs to achieve minimal training loss, which might result in sub-optimal classification performance on the test data with different class distributions. Previous studies addressed the problem by class-resampling[48–51], cost-sensitive learning[52–54]. However, the models with class resampling might overfit the minority categories and underfit the abundant information within the majority categories[54]. Cost-sensitive learning avoids this drawback by directly allocating higher importance to the minority classes than the majority classes[55] while introducing additional training time on hyper-parameter searching[56]. As such, developing a computation-efficient and robust method for multi-label CVDs classification under imbalance class distributions is still an ongoing issue that deserves more attention from future studies.

4 Methods

4.1 Backbone model pre-training

The base backbone model is pre-trained on a public 12-lead ECG dataset (CODE-15%), where 345779 ECG recordings from 233770 patients are provided. The medium and large backbones are pre-trained on a restricted dataset with 2,322,513 ECG recordings from 1,558,772 patients (CODE-full). The specific settings of the backbone models with different sizes are shown in Extended Data Table 2. Note that multiple abnormalities could be identified from one ECG recording simultaneously, which indicates that a multi-label classification model should be implemented for ECG-based CVDs detection. As shown in Fig.1, The backbone model $M(X)$ consists of three parts: (1) Convolution blocks, (2) Self-attention blocks, and (3) Classification blocks. Specifically, the convolution blocks comprise multiple convolution layers (Conv) and batch normalization layers. The Leaky-Relu function is used as the activation function and skip-connection is implemented[57]. In addition, a simple but efficient self-attention pipeline is employed in the self-attention blocks[13] and two successive fully-connected layers with sigmoid activation are used for label prediction in the classification block. A multi-label binary cross-entropy function is employed for model training, defined as,

$$\mathcal{L}(Y, M(X)) = -\frac{1}{BC} \sum_{i=1}^B \sum_{c=1}^C (1 - y_{i,c}) \log(1 - p_{i,c}) + y_{i,c} \log p_{i,c}, \quad (1)$$

where $X = \{x_i\}_{i=1}^B$, $x_i \in \mathbb{R}^{12 \times L}$ are the ECG recordings in the current mini-batch, L is the signal length and $Y = \{y_i\}_{i=1}^B$ is the corresponding ground truths. $p_{i,c}$ is the model prediction on class c and C is the number of categories. During model training, a held-out validation set is used for early-stop model validation. The best-performing model on the validation set is used for downstream tasks on small-scale datasets.

4.2 Random-deactivation low-rank adaptation

Recent studies have demonstrated that low-rank adaptation (LoRA) can drastically decrease computation and storage costs in large-scale neural network fine-tuning while achieving promising performance on downstream tasks[25, 26, 29]. The LoRA method models the incremental update of the pre-trained weights by the matrix multiplication of two low-rank matrices. For a hidden layer output $h = WX$, the LoRA forward process is defined as,

$$h = (W_0 + \Delta W)X = (W_0 + BA)X, \quad (2)$$

where $W_0, \Delta W \in \mathbb{R}^{d_1 \times d_2}$, $B \in \mathbb{R}^{d_1 \times r}$ and $A \in \mathbb{R}^{r \times d_2}$, and the rank $r \ll \min(d_1, d_2)$. The LoRA freezes the pre-trained weight W_0 during model training and only optimizes the low-rank matrices A and B , which greatly reduces the number of trainable parameters during model training[25]. However, the incremental updates of low-rank matrices are inadequate for learning robust representations in downstream tasks[58]. To bridge the performance gap efficiently, we propose a novel random-deactivation low-rank adaptation (RD-LoRA) method, which randomly activates or deactivates the low-rank matrices in each trainable layer with a given probability p . To be specific, the forward process of the proposed RD-LoRA can be defined as,

$$h = (W_0 + \delta BA)X, \delta = \begin{cases} 1, & z \geq p \\ 0, & z < p \end{cases}, \quad (3)$$

where $\delta \sim B(\delta, 1 - p)$ can be regarded as a binary gate controlled by a random variable z following a uniform distribution $U(0, 1)$. In the training stage, the multi-label binary cross-entropy loss defined in Eq.1 is employed for parameter optimization. In the testing stage, for input data X_t and the pre-trained weight

W_0 , the expectation of the output of the RD-LoRA can be given as,

$$\mathbb{E}_{\delta \sim B(\delta, 1-p)} [h_t] = \mathbb{E}_{\delta \sim B(\delta, 1-p)} [(W_0 + \delta BA)X_t]. \quad (4)$$

Considering that the test data X_t is independent from the network parameters, the covariance matrix $Cov(X_t, W_0 + \delta AB)$ equals zero, and thus,

$$\mathbb{E}_{\delta \sim B(\delta, 1-p)} [h_t] = \mathbb{E}_{\delta \sim B(\delta, 1-p)} [(W_0 + \delta BA)X_t] = (\mathbb{E}[W_0] + (1-p)\mathbb{E}[BA])\mathbb{E}[X_t] = (W_0 + (1-p)BA)X_t. \quad (5)$$

Similar to LoRA, the low-rank matrices are merged into the pre-trained weight W_0 in the testing stage to avoid extra inference costs, and the random-drop operation is deactivated. According to Eq.(5), to ensure the expected output will be the same as the output with RD-LoRA, the merged matrix should be computed as,

$$W = W_0 + (1-p)BA. \quad (6)$$

After merging the low-rank matrices into the pre-trained weights of different layers, the final network can be viewed as an ensemble of all possible sub-networks during model training, which improves its stability and generalization performance on unseen test datasets. Additionally, randomly deactivating some low-rank matrices avoids the computation of update matrices in some layers, which improves training speed in the low-rank adaptation of large-scale models.

4.3 Ensemble optimization properties of the RD-LoRA

In this section, we briefly analyze the ensemble properties of the proposed RD-LoRA. Here, we simply consider a network M with n fully-connected layers, defined as $M(X) = \prod_{i=1}^n W_0^i X$, where X is the input data and $W_0^i \in \mathbb{R}^{c_{out} \times c_{in}}$ is the pre-trained weight matrix at the i -th layer. During model training, a convex loss function $\mathcal{L}(Y, M(X))$ is employed for parameter optimization. When the RD-LoRA is activated, the expectation of the loss function $\mathbb{E}_{\delta \sim B(\delta, 1-p)} [\mathcal{L}(Y, M(X))]$ can be given as,

$$(1-p)^n \mathcal{L}(Y, \prod_{i=1}^n (W_0^i + B^i A^i) X) + \sum_{j=1}^n \left[p(1-p)^{n-1} \mathcal{L}(Y, \prod_{i=1, i \neq j}^n (W_0^i + B^i A^i) W_0^j X) \right] + \dots + p^n \mathcal{L}(Y, \prod_{i=1}^n W_0^i X), \quad (7)$$

where the low-rank matrices $\{A^i\}_{i=1}^n$ and $\{B^i\}_{i=1}^n$ are trainable while the pre-trained weights $\{W_0^i\}_{i=1}^n$ are frozen. Eq.(7) can be regarded as a weighted mean of the losses of different sub-networks, which are minimized during model training. The number of activated low-rank matrices of the sub-networks is lower than the entire network. Consequently, the training costs of the sub-networks are lower than those of the entire network. In the testing stage, all the low-rank matrices are merged into the pre-trained weights, which generates an ensemble model combing all the possible sub-networks. The testing loss can be estimated as

$$\mathcal{L}(Y, \mathbb{E}_{\delta \sim B(\delta, 1-p)} [M(X_t)]) = \mathcal{L} \left(Y, \mathbb{E}_{\delta \sim B(\delta, 1-p)} \left[\prod_{i=1}^n (W_0^i + \delta^i B^i A^i) X_t \right] \right) = \mathcal{L}(Y, \prod_{i=1}^n (W_0^i + (1-p)B^i A^i) X_t). \quad (8)$$

In this paper, the multi-label binary cross-entropy loss with sigmoid activation $\sigma(M(X)) = [\sigma(M(X))_1, \sigma(M(X))_2, \dots, \sigma(M(X))_C]$ is convex according to the second-order condition of convexity, where C is the number of categories. Specifically, the Hessian matrix of $\mathcal{L}(Y, \sigma(M(X)))$ is diagonal and the c -th element of the main diagonal can be given as,

$$\begin{aligned} \frac{\partial^2 \mathcal{L}(Y, \sigma(M(X)))}{\partial M(X)_c^2} &= y_c \sigma(M(X))_c (1 - \sigma(M(X))_c) + (1 - y_c) \sigma(M(X))_c (1 - \sigma(M(X))_c) \\ &= \sigma(M(X))_c (1 - \sigma(M(X))_c) \geq 0, \end{aligned} \quad (9)$$

where $Y = [y_1, y_2, \dots, y_C]$, $y_c \in \{0, 1\}$ and $\sigma(M(X)) = (1 + e^{-M(X)})^{-1}$. According to Eq (9), the Hessian matrix of $\mathcal{L}(Y, \sigma(M(X)))$ is positive semidefinite, demonstrating the convexity of the loss function. Based on Jensen's inequality, the loss of any ensemble average is smaller than the average loss of the ensemble components,

$$\mathcal{L}(Y, \mathbb{E}_{\delta \sim B(\delta, 1-p)} [M(X_t)]) \leq \mathbb{E}_{\delta \sim B(\delta, 1-p)} [\mathcal{L}(Y, M(X_t))]. \quad (10)$$

In the training stage, the proposed RD-LoRA optimizes the parameters of multiple sub-networks and generates an ensemble network in the testing stage, improving the model performance on the testing data.

4.4 Efficient one-shot rank allocation

Another limitation of LoRA is that it prespecifies the same rank for all low-rank incremental matrices, neglecting that their importance in model training varies across layers. In response to this limitation, AdaLoRA[30] and IncreLoRA[26] proposed to dynamically adjust the ranks of different incremental matrices during model training based on their importance, which improved the low-rank adaptation performance. However, these dynamic methods require continuous calculation of the importance of all low-rank matrices in each iteration, significantly increasing the computation time. Additionally, their rank allocation processes are based on the singular value decomposition (SVD) theory and thus require an extra regularization loss to force the orthogonality of the low-rank matrices. This property introduces extra hyper-parameters and computation costs. Here, we propose an efficient one-shot rank allocation method to overcome the computation inefficiency of the existing dynamic methods.

Above all, we introduce some preliminaries about how to estimate the importance of weights in neural networks. Based on the first-order Taylor expansion, the importance of a weight matrix can be computed by the error induced by removing it from the network[59], defined as,

$$I(W^i) = \frac{1}{N_e} \sum_{j=1}^{N_e} (\mathcal{L}(Y, M(X)) - \mathcal{L}_{W^i(j)=0}(Y, M(X)))^2 \approx \left\| \frac{\partial \mathcal{L}(Y, M(X))}{\partial W^i} \odot W^i \right\|_2^2, \quad (11)$$

where $W^i(j)$ is the j -th element in the weight matrix W^i , N_e is the number of elements in W^i and \odot is the Hadamard product. However, the gradient matrix $\frac{\partial \mathcal{L}(Y, M(X))}{\partial W^i}$ can not be obtained because W^i is frozen during the low-rank training process. To solve this problem, we approximate it using its incremental update ΔW^i , which can be computed by low-rank matrices A^i and B^i using the Eq.(2).

$$\begin{aligned} \frac{\partial \mathcal{L}(Y, M(X))}{\partial W^i} &\propto -\frac{1}{\eta} \Delta W^i = \frac{1}{\eta} [(W_0^i + B_t^i A_t^i) - (W_0^i + B_{t+1}^i A_{t+1}^i)] = \frac{1}{\eta} (B_t^i A_t^i - B_{t+1}^i A_{t+1}^i) \\ &= \frac{1}{\eta} \left[B_t^i A_t^i - (B_t^i - \eta \frac{\partial \mathcal{L}(Y, M(X))}{\partial B_t^i}) (A_t^i - \eta \frac{\partial \mathcal{L}(Y, M(X))}{\partial A_t^i}) \right] \\ &= B_t^i \frac{\partial \mathcal{L}(Y, M(X))}{\partial A_t^i} + \frac{\partial \mathcal{L}(Y, M(X))}{\partial B_t^i} A_t^i - \eta \frac{\partial \mathcal{L}(Y, M(X))}{\partial B_t^i} \frac{\partial \mathcal{L}(Y, M(X))}{\partial A_t^i}, \end{aligned} \quad (12)$$

where A_t^i and B_t^i are the low-rank matrices at training round t , constant η is the learning rate and W_0 is the pre-trained weight. Although Eq.(12) enables importance score estimation during model training, iterative matrix multiplication induces a heavy computation burden. Hence, we propose to simplify the estimation function Eq.(12) and compute the importance score in a 'one-shot' manner. Specifically, we only use the first gradient-backpropagation process to achieve the entire rank allocation process and fix the ranks of different low-rank matrices during the remaining training iterations. In the first backpropagation process, the low-rank matrices $\{A^i\}_{i=1}^n$ are initialized from a normal distribution $N(0, \sigma^2)$ and $\{B^i\}_{i=1}^n$ are initialized to zero. Consequently, the gradient of $\{A^i\}_{i=1}^n$ at the 0-th (first) iteration is zero according to Eq.(2). Based on the above initialization conditions, Eq.(12) at the 0-th iteration can be rewritten as,

$$\frac{\partial \mathcal{L}(Y, M(X))}{\partial W_0^i} \propto -\frac{1}{\eta} \Delta W_0^i = \frac{\partial \mathcal{L}(Y, M(X))}{\partial B_0^i} A_0^i, \frac{\partial \mathcal{L}(Y, M(X))}{\partial A_0^i} = 0, B_0^i = 0, \quad (13)$$

where $\{W_0^i\}_{i=1}^n$ are the pre-trained weight matrices in the backbone model $M(X)$. Then, the importance score of the pre-trained weight W_0^i can be approximated as,

$$I(W_0^i) \approx \hat{I}(W_0^i) = \left\| \left(\frac{\partial \mathcal{L}(Y, M(X))}{\partial B_0^i} A_0^i \right) \odot W_0^i \right\|_2^2. \quad (14)$$

Then, we sort the importance $\hat{I}(W_0^i)$ of all pre-trained matrices in descending order and allocate different ranks for their low-rank matrices. Here, we assume the ranks of the incremental matrices corresponding to the important weights should be higher than those of the incremental matrices associated with the unimportant weights. The allocated rank r^i of the incremental matrices of the pre-trained weight W_0^i is defined as,

$$r^i = \begin{cases} r, & \hat{I}(W_0^i) \text{ in the top-}k \text{ of } \{\hat{I}(W_0^i)\}_{i=1}^n, k = nc, \\ \frac{1}{2}r, & \text{otherwise} \end{cases} \quad (15)$$

where r is an initial rank, and c is a hyper-parameter that controls the number of important weight matrices. Note that the allocated ranks $\{r^i\}_{i=1}^n$ are fixed during the remaining iterations, and the low-rank

matrices $(\{B^i\}_{i=1}^n, \{A^i\}_{i=1}^n)$ are reset based on their allocated ranks. Eq.(14) is only computed at the 0-th iteration, which avoids numerous matrix multiplication. In addition, the proposed rank allocation process does not require constraint on the orthogonality of low-rank matrices. In summary, the above advantages allow the proposed method to have a faster training speed compared to existing dynamic methods, such as AdaLoRA[30] and IncreLoRA[26].

4.5 Lightweight semi-supervised learning

Semi-supervised learning (SSL) is an efficient tool for model performance enhancement when large-scale unlabeled data is available[7, 60]. Recently, many studies utilized label guessing and consistency regularization to further improve the model performance in SSL tasks, such as FixMatch[8], FlexMatch[21] and SoftMatch[24]. However, the above two techniques require the output predictions of the weak and strong-augmented unlabeled samples, which induces extra computation costs. Consequently, traditional SSL methods usually exhibit much higher memory costs and longer training time than the naive supervised models. Based on the backbone model, we propose a lightweight SSL method without extensive consistency training and pseudo-label guessing.

The main drawback of fully-supervised learning on small datasets is over-fitting, while semi-supervised learning alleviates this problem by utilizing large-scale unlabeled data. However, the heavy computation burden limits their application in real-world scenarios. Consequently, a natural question is: How can we alleviate the over-fitting problem in a lightweight but effective manner? Our solution is to update the batch normalization (BN) layers in a semi-supervised manner using both labeled and unlabeled data. Subsequently, the unlabeled data is released, and only the labeled data is forwarded to the self-attention and classification blocks for loss computation. For labeled inputs $\{x_b^i\}_{i=1}^{N_B}$ and unlabeled inputs $\{x_u^i\}_{i=1}^{N_U}$, the mean value μ and the variance σ of the semi-supervised BN layers in the convolution blocks can be updated as,

$$\mu = \frac{\gamma}{N_B} \sum_{i=1}^{N_B} x_b^i + \frac{1-\gamma}{N_U} \sum_{i=1}^{N_U} x_u^i, \quad (16)$$

$$\sigma = \frac{\gamma}{N_B} \sum_{i=1}^{N_B} (x_b^i - \mu)^2 + \frac{1-\gamma}{N_U} \sum_{i=1}^{N_U} (x_u^i - \mu)^2, \quad (17)$$

where N_B and N_U are the numbers of labeled and unlabeled samples in the current mini-batch, and $\gamma = \frac{N_B}{N_B+N_U}$. Note that N_B equals N_U in this study, thus $\gamma = 0.5$. With very limited labeled data x_b , the estimated mean $\mu_B = \frac{1}{N_B} \sum_{i=1}^{N_B} x_b^i$ and variance $\sigma_B = \frac{1}{N_B} \sum_{i=1}^{N_B} (x_b^i - \mu_B)^2$ in traditional BN are prone to be influenced by the over-fitting problem according to the law of large numbers. On the contrary, the proposed semi-supervised BN alleviates the problem by utilizing large-scale unlabeled data x_u for parameter estimation, which improves the model performance on unseen distributions. Since the BN layers do not exist in the self-attention and classification blocks, we only forward the labeled features to them to reduce memory cost and training time. Although the proposed method discards the label guessing and the consistency regularization modules, the results demonstrate that it achieves similar or even better performance on four datasets than the SOTA SSL methods. Additionally, its computation costs are much lower than the existing methods, including less memory consumption and faster training speed.

4.6 Signal pre-processing and data augmentation

Artifact removal and data augmentation are two factors that play important roles in model performance. Firstly, we introduce the signal pre-processing pipeline employed in the proposed framework. The ECG recordings from the CODE-15% and CODE-full databases are first resampled to a 400Hz sampling rate following the configuration of the dataset provider[5]. The sampling rate of the recordings from the four downstream databases remains unchanged. Subsequently, a band-pass filter (1-47Hz) is applied to remove the power-line interference and baseline drift. Then, the pre-processed signals are normalized using z-score normalization. Secondly, CutMix[61] is employed for labeled data augmentation. Since the sample generation process of CutMix requires true labels that are absent in the unlabeled data, we employed the ECGAugment[10] for unlabeled data augmentation, which generates new samples by randomly selecting a transformation to perturb the pre-processed signals. Note that only the weak-augmentation module in the ECGAugment is employed.

Algorithm 1 FastECG algorithm

Input:

- Labeled dataset $D_B = \{X_b, Y_b\}$ and unlabeled dataset $D_U = \{X_u\}$;
- Pre-trained model $M_0 = \{W_0^i\}_{i=1}^n$; Initial rank r ; The ratio of important weights c ; The random-deactivation probability p ; Batch sizes of the labeled samples (N_B) and the unlabeled samples (N_U).

Output: Adapted model M with the updated parameters $\{W^i = W_0^i + (1 - p)A^i B^i\}_{i=1}^n$;

- 1: One-shot rank allocation
 - 2: Compute the importance of each pre-trained weight using the Eq.(14) and the labeled dataset D_B ;
 - 3: Based on the initial rank r and the ratio c , allocate the final rank r^i of the incremental matrices (A^i, B^i) of the pre-trained weight W_0^i using Eq.(15).
 - 4: **for** 1 to *iteration* **do**
 - 5: sample labeled data $\{x_b, y_b\}$ from D_B ;
 - 6: sample unlabeled data $\{x_u\}$ from D_U ;
 - 7: apply data augmentation to x_b and x_u ;
 - 8: Lightweight semi-supervised learning
 - 9: Based on Eq.(16) and Eq.(17), update the semi-supervised batch-normalization layers in the convolution blocks using the labeled data x_b and the unlabeled data x_u .
 - 10: release the unlabeled data x_u in the GPU memory
 - 11: Random-deactivation low-rank adaptation
 - 12: initialize $h_0 = x_b$
 - 13: **for** $i = 1, 2, \dots, n$ **do**
 - 14: sample δ_i from the Bernoulli distribution $B(\delta, 1 - p)$
 - 15: $h_i = (W_0^i + \delta B^i A^i)h_{i-1}$
 - 16: **end for**
 - 17: Based on the model output h_n and the ground-truth y_b , compute the supervised multi-label binary cross-entropy loss using Eq.(1).
 - 18: apply an early-stop strategy to avoid overfitting;
 - 19: **end for**
 - 20: Merge the incremental matrices into the pre-trained weights, as $\{W^i = W_0^i + (1 - p)B^i A^i\}_{i=1}^n$;
-

5 Data availability

The Georgia 12-lead ECG Challenge (G12EC) database, the Chapman-Shaoxing database, the Ningbo database, and the Physikalisch-Technische Bundesanstalt (PTB-XL) database can be freely downloaded from <https://physionet.org/content/challenge-2021/1.0.3/>. The CODE-15% database is available at <https://zenodo.org/records/4916206>. Restrictions apply to the availability of the CODE-full database, and requests to access it must be submitted and reviewed individually by the Telehealth Network of Minas Gerais (antonio.ribeiro@ebserh.gov.br) for academic use only.

6 Code availability

All relevant models were implemented based on Python language and a popular deep-learning framework Pytorch. The source code and the pre-trained backbones can be found at <https://github.com/KAZABANA/FastECG>.

References

- [1] Kelly, B. B., Fuster, V. *et al.* *Promoting cardiovascular health in the developing world: a critical challenge to achieve global health* (National Academies Press, 2010).
- [2] Kiyasseh, D., Zhu, T. & Clifton, D. A clinical deep learning framework for continually learning from cardiac signals across diseases, time, modalities, and institutions. *Nature Communications* **12**, 4221 (2021).
- [3] Lai, J. *et al.* Practical intelligent diagnostic algorithm for wearable 12-lead ECG via self-supervised learning on large-scale dataset. *Nature Communications* **14**, 3741 (2023).
- [4] Hannun, A. Y. *et al.* Cardiologist-level arrhythmia detection and classification in ambulatory electrocardiograms using a deep neural network. *Nature medicine* **25**, 65–69 (2019).

- [5] Ribeiro, A. H. *et al.* Automatic diagnosis of the 12-lead ECG using a deep neural network. *Nature communications* **11**, 1760 (2020).
- [6] Al-Zaiti, S. S. *et al.* Machine learning for ecg diagnosis and risk stratification of occlusion myocardial infarction. *Nature Medicine* **29**, 1804–1813 (2023).
- [7] Berthelot, D. *et al.* Mixmatch: A holistic approach to semi-supervised learning (2019).
- [8] Sohn, K. *et al.* Fixmatch: Simplifying semi-supervised learning with consistency and confidence (2020).
- [9] Zhang, P. *et al.* Semi-supervised learning for automatic atrial fibrillation detection in 24-hour holter monitoring. *IEEE Journal of Biomedical and Health Informatics* **26**, 3791–3801 (2022).
- [10] Zhou, R. *et al.* Semi-supervised learning for multi-label cardiovascular diseases prediction: A multi-dataset study. *IEEE Transactions on Pattern Analysis and Machine Intelligence* 1–17 (2023).
- [11] Houshy, N. *et al.* Parameter-efficient transfer learning for nlp (2019).
- [12] Vaswani, A. *et al.* Attention is all you need. *Advances in neural information processing systems* **30** (2017).
- [13] Radford, A. *et al.* Language models are unsupervised multitask learners (2019).
- [14] He, K. *et al.* Masked autoencoders are scalable vision learners (2022).
- [15] El-Nouby, A. *et al.* Scalable pre-training of large autoregressive image models. *arXiv preprint arXiv:2401.08541* (2024).
- [16] Kiyasseh, D., Zhu, T. & Clifton, D. A. Clocs: Contrastive learning of cardiac signals across space, time, and patients (2021).
- [17] Vaid, A. *et al.* A foundational vision transformer improves diagnostic performance for electrocardiograms. *NPJ Digital Medicine* **6**, 108 (2023).
- [18] Wang, X., Gao, J., Long, M. & Wang, J. Meila, M. & Zhang, T. (eds) *Self-tuning for data-efficient deep learning*. (eds Meila, M. & Zhang, T.) *Proceedings of the 38th International Conference on Machine Learning*, Vol. 139 of *Proceedings of Machine Learning Research*, 10738–10748 (PMLR, 2021). URL <https://proceedings.mlr.press/v139/wang21g.html>.
- [19] Zhou, H.-Y., Oliver, A., Wu, J. & Zheng, Y. When semi-supervised learning meets transfer learning: Training strategies, models and datasets. *arXiv preprint arXiv:1812.05313* (2018).
- [20] Li, J., Xiong, C. & Hoi, S. C. Comatch: Semi-supervised learning with contrastive graph regularization (2021).
- [21] Zhang, B. *et al.* Flexmatch: Boosting semi-supervised learning with curriculum pseudo labeling (2021).
- [22] Peiris, H., Hayat, M., Chen, Z., Egan, G. & Harandi, M. Uncertainty-guided dual-views for semi-supervised volumetric medical image segmentation. *Nature Machine Intelligence* **5**, 724–738 (2023).
- [23] Berthelot, D. *et al.* Remixmatch: Semi-supervised learning with distribution matching and augmentation anchoring (2020).
- [24] Chen, H. *et al.* Softmatch: Addressing the quantity-quality tradeoff in semi-supervised learning (2023).
- [25] Hu, E. J. *et al.* LoRA: Low-rank adaptation of large language models (2022). URL <https://openreview.net/forum?id=nZeVKeeFYf9>.
- [26] Zhang, Q. *et al.* Adaptive budget allocation for parameter-efficient fine-tuning (2023). URL <https://openreview.net/forum?id=lq62uWRJjiY>.
- [27] Zaken, E. B., Ravfogel, S. & Goldberg, Y. Bitfit: Simple parameter-efficient fine-tuning for transformer-based masked language-models. *arXiv preprint arXiv:2106.10199* (2021).

- [28] Chen, Y. *et al.* Hadamard adapter: An extreme parameter-efficient adapter tuning method for pre-trained language models (2023).
- [29] Ding, N. *et al.* Parameter-efficient fine-tuning of large-scale pre-trained language models. *Nature Machine Intelligence* **5**, 220–235 (2023).
- [30] Zhang, F. *et al.* Increlora: Incremental parameter allocation method for parameter-efficient fine-tuning. *arXiv preprint arXiv:2308.12043* (2023).
- [31] Ribeiro, A. L. P. *et al.* Tele-electrocardiography and bigdata: the code (clinical outcomes in digital electrocardiography) study. *Journal of electrocardiology* **57**, S75–S78 (2019).
- [32] Lu, L. *et al.* Decoding 2.3 million ECGs: interpretable deep learning for advancing cardiovascular diagnosis and mortality risk stratification. *European Heart Journal - Digital Health* ztae014 (2024). URL <https://doi.org/10.1093/ehjdh/ztae014>.
- [33] Alday, E. A. P. *et al.* Classification of 12-lead ECGs: the physionet/computing in cardiology challenge 2020. *Physiological measurement* **41**, 124003 (2020).
- [34] Zheng, J. *et al.* A 12-lead electrocardiogram database for arrhythmia research covering more than 10,000 patients. *Scientific data* **7**, 48 (2020).
- [35] Zheng, J. *et al.* Optimal multi-stage arrhythmia classification approach. *Scientific reports* **10**, 2898 (2020).
- [36] Wagner, P. *et al.* PTB-XL, a large publicly available electrocardiography dataset. *Scientific data* **7**, 154 (2020).
- [37] Loshchilov, I. & Hutter, F. Decoupled weight decay regularization. *arXiv preprint arXiv:1711.05101* (2017).
- [38] Guo, L.-Z. & Li, Y.-F. Class-imbalanced semi-supervised learning with adaptive thresholding (2022).
- [39] Lai, Z., Wang, C., Gunawan, H., Cheung, S.-C. S. & Chuah, C.-N. Smoothed adaptive weighting for imbalanced semi-supervised learning: Improve reliability against unknown distribution data (2022).
- [40] Valipour, M., Rezagholizadeh, M., Kobzyev, I. & Ghodsi, A. Vlachos, A. & Augenstein, I. (eds) *DyLoRA: Parameter-efficient tuning of pre-trained models using dynamic search-free low-rank adaptation*. (eds Vlachos, A. & Augenstein, I.) *Proceedings of the 17th Conference of the European Chapter of the Association for Computational Linguistics*, 3274–3287 (Association for Computational Linguistics, Dubrovnik, Croatia, 2023). URL <https://aclanthology.org/2023.eacl-main.239>.
- [41] Strodthoff, N., Wagner, P., Schaeffter, T. & Samek, W. Deep learning for ECG analysis: Benchmarks and insights from PTB-XL. *IEEE Journal of Biomedical and Health Informatics* **25**, 1519–1528 (2020).
- [42] Li, X. L. & Liang, P. Prefix-tuning: Optimizing continuous prompts for generation. *arXiv preprint arXiv:2101.00190* (2021).
- [43] Dosovitskiy, A. *et al.* An image is worth 16x16 words: Transformers for image recognition at scale. *arXiv preprint arXiv:2010.11929* (2020).
- [44] Liu, Z. *et al.* Swin transformer: Hierarchical vision transformer using shifted windows (2021).
- [45] Zhai, X., Zhou, Z. & Tin, C. Semi-supervised learning for ECG classification without patient-specific labeled data. *Expert Systems with Applications* **158**, 113411 (2020).
- [46] Oliveira, L. C., Lai, Z., Siefkes, H. M. & Chuah, C.-N. Generalizable semi-supervised learning strategies for multiple learning tasks using 1-D biomedical signals.
- [47] Verma, V. *et al.* Interpolation consistency training for semi-supervised learning. *Neural Networks* **145**, 90–106 (2022). URL <https://www.sciencedirect.com/science/article/pii/S0893608021003993>.
- [48] He, H. & Garcia, E. A. Learning from imbalanced data. *IEEE Transactions on knowledge and data engineering* **21**, 1263–1284 (2009).

- [49] Shen, L., Lin, Z. & Huang, Q. Relay backpropagation for effective learning of deep convolutional neural networks (2016).
- [50] Buda, M., Maki, A. & Mazurowski, M. A. A systematic study of the class imbalance problem in convolutional neural networks. *Neural networks* **106**, 249–259 (2018).
- [51] Kang, B. *et al.* Decoupling representation and classifier for long-tailed recognition. *arXiv preprint arXiv:1910.09217* (2019).
- [52] Huang, C., Li, Y., Loy, C. C. & Tang, X. Learning deep representation for imbalanced classification (2016).
- [53] Cui, Y., Jia, M., Lin, T.-Y., Song, Y. & Belongie, S. Class-balanced loss based on effective number of samples (2019).
- [54] Wu, T., Huang, Q., Liu, Z., Wang, Y. & Lin, D. Distribution-balanced loss for multi-label classification in long-tailed datasets (2020).
- [55] Ben-Baruch, E. *et al.* Asymmetric loss for multi-label classification (2020). [2009.14119](https://arxiv.org/abs/2009.14119).
- [56] Du, J., Zhou, Y., Liu, P., Vong, C.-M. & Wang, T. Parameter-free loss for class-imbalanced deep learning in image classification. *IEEE Transactions on Neural Networks and Learning Systems* **34**, 3234–3240 (2023).
- [57] Nejedly, P. *et al.* Classification of ECG using ensemble of residual CNNs with attention mechanism (2021).
- [58] Zi, B. *et al.* Delta-lora: Fine-tuning high-rank parameters with the delta of low-rank matrices. *arXiv preprint arXiv:2309.02411* (2023).
- [59] Molchanov, P., Mallya, A., Tyree, S., Frosio, I. & Kautz, J. Importance estimation for neural network pruning (2019).
- [60] Chapelle, O., Schölkopf, B. & Zien, A. *Semi-Supervised Learning* Vol. 2 (The MIT Press, 2006).
- [61] Yun, S. *et al.* Cutmix: Regularization strategy to train strong classifiers with localizable features (2019).

Acknowledgments. This work was supported by an RAEng Research Chair, the InnoHK Hong Kong projects under the Hong Kong Center for Cerebro-cardiovascular Health Engineering (COCHE), the National Natural Science Foundation of China (22322816) and the City University of Hong Kong Project (9610640).

Author contributions. R.Z. and Y.D. conceived and designed the study. R.Z. wrote the code and conducted the experiments. Z.L. helped to prepare figures and tables. R.Z. and Y.D. co-wrote the manuscript. L.C. helped to revise the manuscript. Y.D., K.W.Y.C., D.A.C., and Y.Z. were senior advisors to the project. All authors contributed to results interpretation and final manuscript preparation.

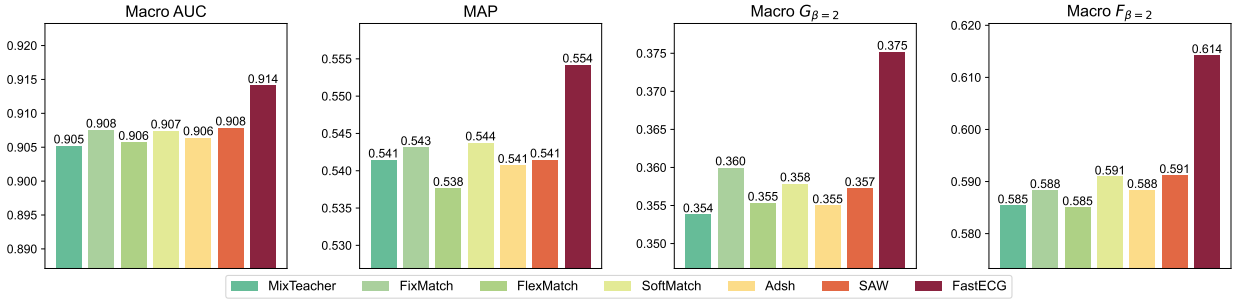
Competing interests. The authors declare that they have no conflicts of interest.

Extended Data Table 1: Performance comparisons between FastECG and parameter-efficient semi-supervised baselines on the base backbone. The average performance on all CVDs within each dataset is shown across six seeds. The standard deviation is also reported for the evaluation metrics.

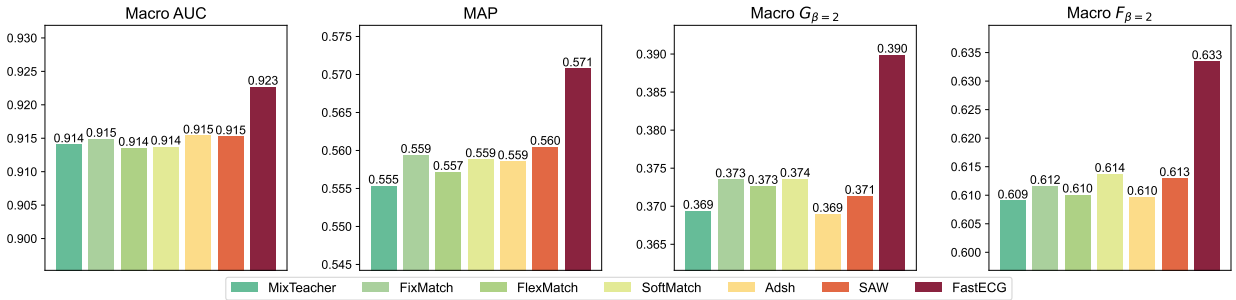
Methods	Params ↓	Time/iter ↓	Ranking Loss ↓	Coverage ↓	Macro AUC ↑	MAP ↑	Macro $G_{\beta=2}$ ↑	Macro $F_{\beta=2}$ ↑
G12EC Dataset								
FixMatch	9.505 M	187 ms	0.107±0.006	4.292±0.163	0.829±0.004	0.468±0.009	0.280±0.010	0.510±0.016
+ LoRA _{r=16}	0.795 M	204 ms	0.098±0.003	4.003±0.114	0.841±0.009	0.460±0.017	0.279±0.022	0.518±0.031
+ DyLoRA _{r=16}	0.795 M	204 ms	0.098±0.004	3.981±0.084	0.841±0.009	0.456±0.010	0.282±0.017	0.515±0.022
+ AdaLoRA _{r=16}	0.796 M	237 ms	0.096±0.003	3.986±0.110	0.844±0.007	0.461±0.008	0.284±0.015	0.520±0.015
+ InceLoRA _{r=16}	0.824 M	430 ms	0.088±0.003	3.770±0.056	0.850±0.005	0.460±0.008	0.289±0.011	0.532±0.013
+ LoRA _{r=4}	0.222 M	202 ms	0.092±0.004	3.859±0.124	0.850±0.007	0.467±0.004	0.289±0.014	0.529±0.024
+ DyLoRA _{r=4}	0.222 M	203 ms	0.095±0.002	3.915±0.106	0.843±0.005	0.460±0.009	0.278±0.017	0.518±0.016
+ AdaLoRA _{r=4}	0.222 M	236 ms	0.093±0.003	3.871±0.079	0.849±0.005	0.463±0.008	0.288±0.011	0.528±0.016
+ InceLoRA _{r=4}	0.246 M	292 ms	0.090±0.001	3.817±0.043	0.847±0.005	0.454±0.006	0.281±0.015	0.521±0.022
FastECG_{r=16}	0.510 M	98 ms	0.092±0.002	3.867±0.088	0.855±0.005	0.476±0.006	0.307±0.016	0.551±0.017
FastECG_{r=4}	0.183 M	98 ms	0.089±0.003	3.804±0.095	0.853±0.004	0.467±0.006	0.304±0.013	0.553±0.020
PTB-XL Dataset								
FixMatch	9.505 M	208 ms	0.038±0.001	2.905±0.061	0.882±0.004	0.510±0.006	0.322±0.007	0.541±0.007
+ LoRA _{r=16}	0.795 M	225 ms	0.033±0.001	2.733±0.034	0.892±0.002	0.520±0.006	0.331±0.005	0.557±0.004
+ DyLoRA _{r=16}	0.795 M	226 ms	0.033±0.001	2.716±0.057	0.894±0.003	0.524±0.003	0.321±0.010	0.553±0.010
+ AdaLoRA _{r=16}	0.796 M	262 ms	0.032±0.001	2.687±0.025	0.896±0.003	0.508±0.009	0.326±0.012	0.552±0.015
+ InceLoRA _{r=16}	0.825 M	469 ms	0.031±0.001	2.620±0.020	0.903±0.002	0.520±0.004	0.342±0.008	0.573±0.008
+ LoRA _{r=4}	0.222 M	225 ms	0.032±0.001	2.673±0.035	0.898±0.004	0.522±0.006	0.329±0.012	0.554±0.009
+ DyLoRA _{r=4}	0.222 M	225 ms	0.032±0.001	2.668±0.036	0.896±0.003	0.521±0.005	0.328±0.008	0.554±0.008
+ AdaLoRA _{r=4}	0.223 M	263 ms	0.032±0.000	2.696±0.010	0.896±0.002	0.510±0.003	0.323±0.008	0.550±0.012
+ InceLoRA _{r=4}	0.246 M	322 ms	0.031±0.001	2.630±0.034	0.899±0.004	0.518±0.006	0.338±0.009	0.570±0.010
FastECG_{r=16}	0.582 M	110 ms	0.031±0.000	2.641±0.020	0.901±0.003	0.530±0.005	0.346±0.006	0.578±0.006
FastECG_{r=4}	0.159 M	109 ms	0.030±0.001	2.626±0.026	0.899±0.004	0.526±0.005	0.346±0.005	0.580±0.006
Ningbo Dataset								
FixMatch	9.506 M	217 ms	0.035±0.003	3.025±0.121	0.922±0.009	0.493±0.023	0.321±0.014	0.545±0.020
+ LoRA _{r=16}	0.796 M	234 ms	0.032±0.001	2.864±0.045	0.926±0.002	0.497±0.018	0.326±0.007	0.561±0.008
+ DyLoRA _{r=16}	0.796 M	235 ms	0.032±0.002	2.874±0.083	0.927±0.003	0.498±0.017	0.321±0.011	0.553±0.016
+ AdaLoRA _{r=16}	0.797 M	272 ms	0.032±0.002	2.851±0.054	0.925±0.003	0.487±0.021	0.317±0.017	0.546±0.028
+ InceLoRA _{r=16}	0.827 M	491 ms	0.030±0.001	2.772±0.045	0.929±0.003	0.499±0.023	0.328±0.011	0.564±0.016
+ LoRA _{r=4}	0.223 M	234 ms	0.031±0.001	2.842±0.046	0.926±0.003	0.489±0.026	0.319±0.013	0.551±0.019
+ DyLoRA _{r=4}	0.223 M	234 ms	0.031±0.001	2.841±0.034	0.924±0.003	0.489±0.020	0.323±0.016	0.556±0.026
+ AdaLoRA _{r=4}	0.224 M	272 ms	0.033±0.001	2.896±0.037	0.923±0.004	0.480±0.018	0.312±0.006	0.543±0.017
+ InceLoRA _{r=4}	0.247 M	332 ms	0.030±0.001	2.794±0.046	0.927±0.002	0.490±0.025	0.314±0.014	0.551±0.022
FastECG_{r=16}	0.550 M	115 ms	0.030±0.001	2.805±0.063	0.928±0.002	0.505±0.019	0.334±0.011	0.569±0.014
FastECG_{r=4}	0.168 M	114 ms	0.030±0.001	2.776±0.028	0.929±0.001	0.500±0.017	0.327±0.010	0.567±0.011
Chapman Dataset								
FixMatch	9.504 M	186 ms	0.046±0.004	2.626±0.096	0.897±0.006	0.520±0.009	0.339±0.012	0.518±0.025
+ LoRA _{r=16}	0.795 M	201 ms	0.041±0.002	2.493±0.058	0.899±0.005	0.521±0.014	0.338±0.011	0.515±0.015
+ DyLoRA _{r=16}	0.795 M	202 ms	0.042±0.004	2.512±0.091	0.899±0.003	0.524±0.011	0.336±0.009	0.511±0.015
+ AdaLoRA _{r=16}	0.795 M	234 ms	0.042±0.001	2.520±0.039	0.883±0.011	0.503±0.020	0.338±0.018	0.498±0.019
+ InceLoRA _{r=16}	0.822 M	426 ms	0.041±0.003	2.484±0.072	0.884±0.017	0.495±0.022	0.334±0.019	0.504±0.029
+ LoRA _{r=4}	0.222 M	201 ms	0.038±0.001	2.427±0.039	0.902±0.006	0.522±0.010	0.338±0.011	0.523±0.012
+ DyLoRA _{r=4}	0.222 M	200 ms	0.039±0.002	2.445±0.057	0.898±0.010	0.518±0.013	0.331±0.008	0.506±0.016
+ AdaLoRA _{r=4}	0.222 M	233 ms	0.039±0.002	2.457±0.044	0.891±0.010	0.512±0.014	0.345±0.014	0.521±0.018
+ InceLoRA _{r=4}	0.246 M	288 ms	0.039±0.001	2.446±0.039	0.888±0.008	0.502±0.015	0.339±0.014	0.505±0.022
FastECG_{r=16}	0.581 M	97 ms	0.040±0.002	2.483±0.055	0.896±0.006	0.536±0.004	0.355±0.005	0.530±0.008
FastECG_{r=4}	0.180 M	97 ms	0.038±0.002	2.418±0.049	0.898±0.005	0.526±0.006	0.352±0.009	0.530±0.012

Extended Data Table 2: Backbone model specifications. N_{conv} indicates the number of convolution blocks, N_{att} indicates the number of self-attention blocks, and N_{cls} indicates the number of classification blocks. C is the number of convolution channels. Hidden size is the hidden layer dimension of the self-attention blocks. Head Num is the number of heads in multi-head self-attention. Params is the total number of parameters in the backbone.

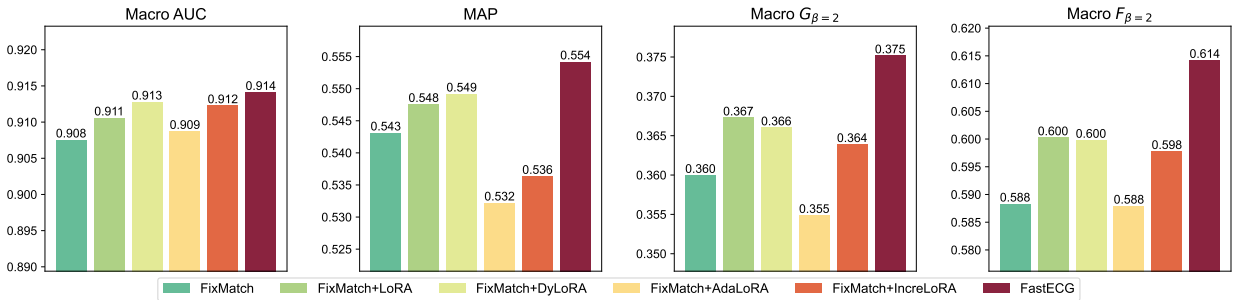
Backbone Size	N_{conv}	N_{att}	N_{cls}	C	Hidden size	Head Num	Params
Base	3	8	1	256	256	16	9.505M
Medium	3	12	1	512	512	16	50.494M
Large	3	12	1	768	768	16	113.490M



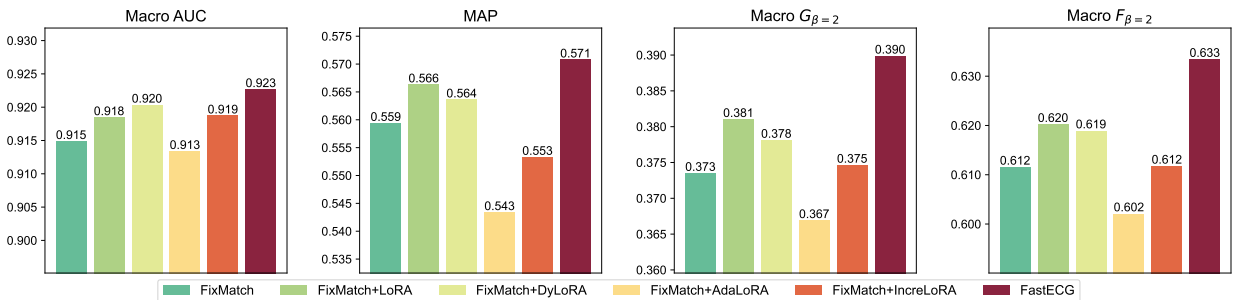
(a) Comparisons between FastECG and semi-supervised baselines (labeled ratio = 0.10)



(b) Comparisons between FastECG and semi-supervised baselines (labeled ratio = 0.15)

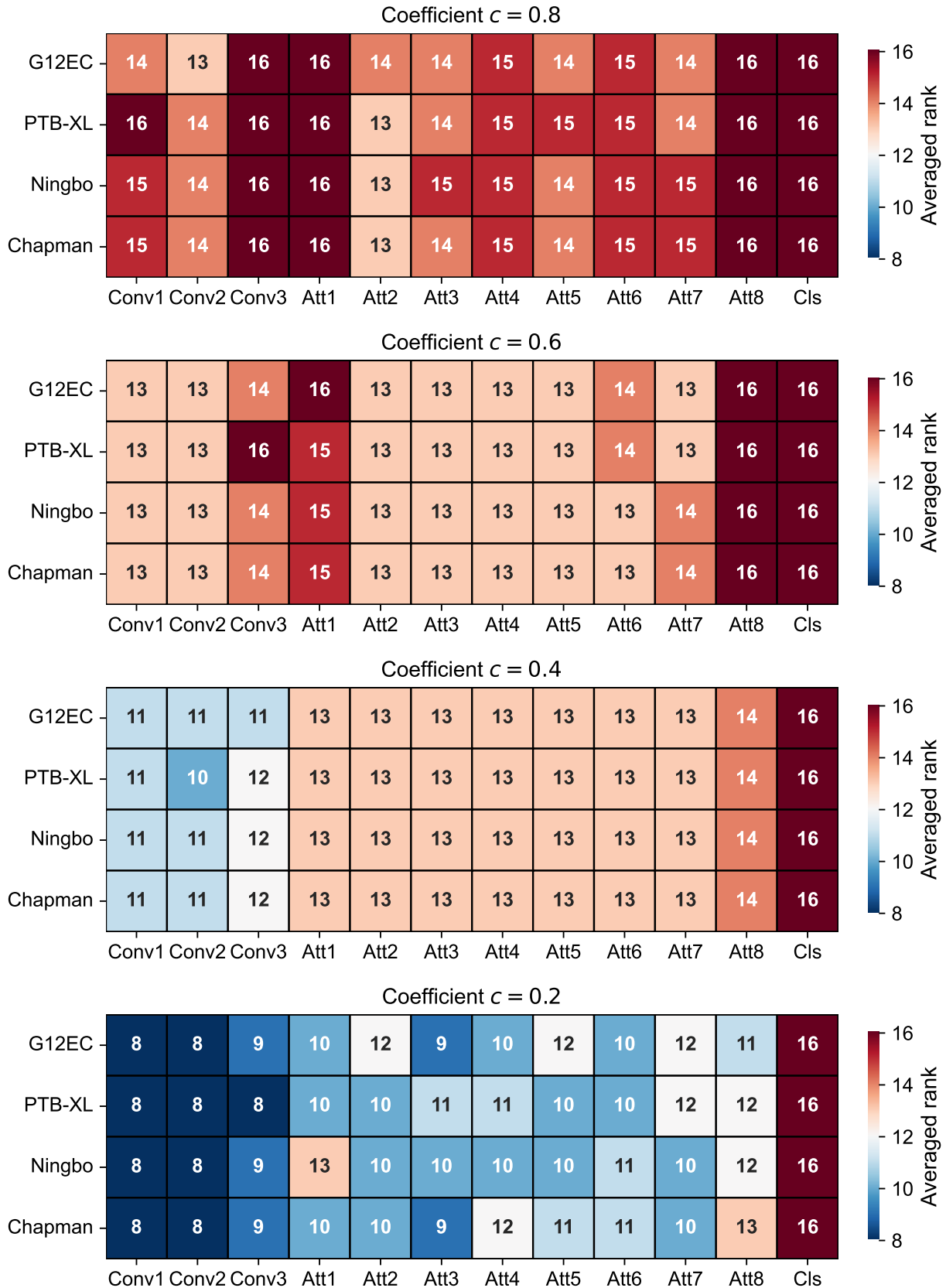


(c) Comparisons between FastECG and parameter-efficient semi-supervised baselines (labeled ratio = 0.10)



(d) Comparisons between FastECG and parameter-efficient semi-supervised baselines (labeled ratio = 0.15)

Extended Data Fig. 1: Performance comparisons between FastECG and the baseline models under various labeled ratios using the base backbone.



Extended Data Fig. 2: The rank distributions generated by the proposed one-shot rank allocation method on four datasets using the base backbone. Specifically, we visualize the allocated rank of each block in the backbone network, which is the average rank of the incremental matrices within the block. For simplicity, we present the abbreviations of different blocks. ('Conv1': the 1-st convolution block; 'Att1': the 1-st self-attention block ; 'Cls': classification block).

Extended Data Table 3: Performance comparisons between FastECG and semi-supervised baselines on the medium backbone. The average performance on all CVDs within each dataset is shown across six seeds. The standard deviation is also reported for the evaluation metrics.

Methods	Params ↓	Mem ↓	Time/iter ↓	Ranking Loss ↓	Coverage ↓	Macro AUC ↑	MAP ↑	Macro $G_{\beta=2}$ ↑	Macro $F_{\beta=2}$ ↑
G12EC Dataset									
ReMixMatch	50.493 M	17.931 GB	719 ms	0.160±0.009	5.299±0.175	0.766±0.014	0.318±0.020	0.194±0.013	0.430±0.023
MixedTeacher	50.493 M	9.461 GB	396 ms	0.096±0.003	4.016±0.060	0.846±0.008	0.499±0.009	0.303±0.014	0.537±0.018
FixMatch	50.493 M	13.589 GB	499 ms	0.096±0.006	4.027±0.109	0.850±0.009	0.499±0.014	0.299±0.016	0.529±0.016
FlexMatch	50.493 M	13.589 GB	498 ms	0.104±0.003	4.216±0.070	0.848±0.008	0.499±0.009	0.294±0.019	0.521±0.020
SoftMatch	50.493 M	13.589 GB	498 ms	0.097±0.003	4.096±0.093	0.853±0.007	0.505±0.008	0.309±0.010	0.536±0.013
Adsh	50.493 M	9.251 GB	524 ms	0.098±0.003	4.107±0.090	0.845±0.008	0.493±0.011	0.298±0.014	0.531±0.020
SAW	50.493 M	13.589 GB	499 ms	0.100±0.003	4.129±0.083	0.847±0.004	0.490±0.007	0.293±0.014	0.526±0.012
FastECG_{r=16}	1.568 M	6.158 GB	243 ms	0.086±0.004	3.740±0.134	0.862±0.006	0.507±0.007	0.317±0.022	0.561±0.024
FastECG_{r=4}	0.458 M	6.146 GB	241 ms	0.085±0.002	3.741±0.068	0.862±0.007	0.503±0.006	0.316±0.013	0.560±0.015
PTB-XL Dataset									
ReMixMatch	50.494 M	17.931 GB	797 ms	0.064±0.005	3.589±0.161	0.815±0.012	0.335±0.017	0.209±0.010	0.423±0.009
MixedTeacher	50.494 M	9.459 GB	440 ms	0.032±0.001	2.706±0.049	0.898±0.004	0.539±0.005	0.340±0.013	0.559±0.012
FixMatch	50.494 M	13.589 GB	553 ms	0.034±0.002	2.767±0.053	0.898±0.003	0.536±0.006	0.340±0.006	0.556±0.010
FlexMatch	50.494 M	13.589 GB	553 ms	0.034±0.001	2.747±0.047	0.901±0.004	0.529±0.004	0.348±0.013	0.559±0.008
SoftMatch	50.494 M	13.589 GB	553 ms	0.034±0.001	2.790±0.026	0.898±0.003	0.533±0.004	0.341±0.007	0.553±0.009
Adsh	50.494 M	9.251 GB	796 ms	0.033±0.002	2.757±0.079	0.901±0.003	0.537±0.007	0.339±0.008	0.557±0.014
SAW	50.494 M	13.589 GB	554 ms	0.034±0.001	2.778±0.050	0.899±0.001	0.531±0.010	0.344±0.011	0.562±0.009
FastECG_{r=16}	1.485 M	6.161 GB	271 ms	0.027±0.001	2.539±0.033	0.913±0.003	0.550±0.004	0.369±0.005	0.588±0.003
FastECG_{r=4}	0.505 M	6.150 GB	270 ms	0.027±0.001	2.529±0.019	0.914±0.003	0.547±0.003	0.372±0.006	0.599±0.010
Ningbo Dataset									
ReMixMatch	50.496 M	17.932 GB	825 ms	0.082±0.016	4.224±0.386	0.829±0.025	0.298±0.038	0.195±0.027	0.396±0.034
MixedTeacher	50.496 M	9.459 GB	457 ms	0.031±0.002	2.856±0.078	0.926±0.009	0.525±0.023	0.342±0.016	0.571±0.023
FixMatch	50.496 M	13.589 GB	572 ms	0.031±0.002	2.869±0.081	0.931±0.003	0.531±0.021	0.349±0.014	0.575±0.015
FlexMatch	50.496 M	13.589 GB	573 ms	0.031±0.002	2.853±0.081	0.930±0.002	0.524±0.012	0.347±0.013	0.575±0.018
SoftMatch	50.496 M	13.589 GB	574 ms	0.031±0.002	2.877±0.094	0.927±0.002	0.525±0.019	0.344±0.014	0.573±0.017
Adsh	50.496 M	9.251 GB	1061 ms	0.031±0.002	2.868±0.061	0.927±0.004	0.523±0.013	0.342±0.012	0.571±0.017
SAW	50.496 M	13.589 GB	572 ms	0.032±0.002	2.911±0.105	0.930±0.003	0.525±0.017	0.342±0.013	0.578±0.016
FastECG_{r=16}	1.705 M	6.172 GB	282 ms	0.027±0.001	2.701±0.051	0.933±0.003	0.531±0.018	0.356±0.013	0.588±0.021
FastECG_{r=4}	0.507 M	6.160 GB	282 ms	0.026±0.001	2.661±0.058	0.934±0.004	0.525±0.018	0.352±0.013	0.587±0.020
Chapman Dataset									
ReMixMatch	50.492 M	17.931 GB	715 ms	0.101±0.019	3.608±0.283	0.823±0.021	0.362±0.036	0.230±0.029	0.426±0.028
MixedTeacher	50.492 M	9.461 GB	394 ms	0.037±0.002	2.420±0.071	0.909±0.010	0.539±0.007	0.348±0.016	0.513±0.026
FixMatch	50.492 M	13.589 GB	495 ms	0.038±0.004	2.439±0.092	0.905±0.010	0.538±0.011	0.357±0.009	0.522±0.020
FlexMatch	50.492 M	13.589 GB	495 ms	0.041±0.003	2.519±0.077	0.901±0.004	0.531±0.011	0.345±0.016	0.512±0.030
SoftMatch	50.492 M	13.589 GB	495 ms	0.043±0.004	2.546±0.101	0.902±0.009	0.535±0.008	0.355±0.015	0.526±0.026
Adsh	50.492 M	9.251 GB	527 ms	0.039±0.004	2.440±0.073	0.909±0.006	0.546±0.007	0.356±0.007	0.530±0.013
SAW	50.492 M	13.589 GB	493 ms	0.043±0.003	2.549±0.073	0.901±0.006	0.531±0.008	0.357±0.013	0.532±0.027
FastECG_{r=16}	1.601 M	6.159 GB	241 ms	0.035±0.002	2.362±0.049	0.909±0.007	0.553±0.013	0.367±0.008	0.540±0.019
FastECG_{r=4}	0.402 M	6.145 GB	240 ms	0.034±0.001	2.334±0.033	0.908±0.008	0.538±0.014	0.361±0.009	0.531±0.019

Extended Data Table 4: Performance comparisons between FastECG and semi-supervised baselines on the large backbone. The average performance on all CVDs within each dataset is shown across six seeds. The standard deviation is also reported for the evaluation metrics.

Methods	Params ↓	Mem ↓	Time/iter ↓	Ranking Loss ↓	Coverage ↓	Macro AUC ↑	MAP ↑	Macro $G_{\beta=2}$ ↑	Macro $F_{\beta=2}$ ↑
G12EC Dataset									
ReMixMatch	113.489 M	26.325 GB	1418 ms	0.157±0.016	5.240±0.328	0.776±0.017	0.336±0.025	0.205±0.019	0.432±0.027
MixedTeacher	113.489 M	14.257 GB	728 ms	0.111±0.022	4.365±0.447	0.835±0.026	0.489±0.018	0.285±0.017	0.517±0.029
FixMatch	113.489 M	20.061 GB	966 ms	0.100±0.005	4.147±0.113	0.843±0.007	0.493±0.008	0.293±0.011	0.518±0.015
FlexMatch	113.489 M	20.061 GB	966 ms	0.099±0.006	4.088±0.149	0.847±0.003	0.489±0.005	0.299±0.011	0.534±0.015
SoftMatch	113.489 M	20.061 GB	943 ms	0.100±0.007	4.138±0.194	0.847±0.004	0.498±0.005	0.297±0.004	0.532±0.013
Adsh	113.489 M	13.815 GB	951 ms	0.103±0.003	4.240±0.073	0.843±0.008	0.496±0.007	0.294±0.010	0.521±0.023
SAW	113.489 M	20.061 GB	939 ms	0.102±0.002	4.189±0.070	0.842±0.003	0.490±0.005	0.300±0.007	0.534±0.019
FastECG_{r=16}	2.658 M	9.217 GB	453 ms	0.085±0.005	3.778±0.140	0.857±0.004	0.509±0.007	0.322±0.009	0.565±0.010
FastECG_{r=4}	0.761 M	9.206 GB	453 ms	0.084±0.003	3.742±0.117	0.859±0.004	0.506±0.007	0.323±0.004	0.561±0.002
PTB-XL Dataset									
ReMixMatch	113.490 M	26.325 GB	1614 ms	0.063±0.011	3.590±0.332	0.834±0.024	0.380±0.029	0.237±0.027	0.449±0.033
MixedTeacher	113.490 M	14.257 GB	809 ms	0.035±0.001	2.831±0.032	0.895±0.006	0.522±0.004	0.334±0.006	0.556±0.008
FixMatch	113.490 M	20.061 GB	1072 ms	0.035±0.003	2.805±0.102	0.894±0.004	0.521±0.006	0.342±0.007	0.560±0.012
FlexMatch	113.490 M	20.061 GB	1071 ms	0.041±0.004	3.016±0.124	0.893±0.004	0.519±0.006	0.342±0.010	0.557±0.010
SoftMatch	113.490 M	20.061 GB	1047 ms	0.038±0.003	2.886±0.094	0.893±0.004	0.523±0.007	0.334±0.007	0.542±0.011
Adsh	113.490 M	13.815 GB	1432 ms	0.036±0.003	2.848±0.114	0.892±0.002	0.527±0.005	0.343±0.009	0.563±0.010
SAW	113.490 M	20.061 GB	1039 ms	0.035±0.002	2.825±0.068	0.899±0.006	0.532±0.006	0.347±0.007	0.560±0.010
FastECG_{r=16}	2.235 M	9.220 GB	508 ms	0.030±0.002	2.618±0.061	0.909±0.004	0.537±0.004	0.358±0.005	0.587±0.008
FastECG_{r=4}	0.712 M	9.211 GB	506 ms	0.029±0.001	2.602±0.028	0.908±0.003	0.535±0.004	0.356±0.006	0.582±0.008
Ningbo Dataset									
ReMixMatch	113.493 M	26.325 GB	1637 ms	0.069±0.012	3.949±0.262	0.863±0.011	0.339±0.026	0.226±0.017	0.442±0.021
MixedTeacher	113.493 M	14.257 GB	840 ms	0.033±0.002	2.934±0.079	0.929±0.003	0.518±0.021	0.341±0.018	0.572±0.026
FixMatch	113.493 M	20.061 GB	1111 ms	0.033±0.002	2.962±0.070	0.926±0.004	0.513±0.024	0.337±0.018	0.563±0.027
FlexMatch	113.493 M	20.061 GB	1083 ms	0.035±0.002	3.038±0.076	0.926±0.004	0.511±0.023	0.332±0.012	0.562±0.017
SoftMatch	113.493 M	20.061 GB	1080 ms	0.034±0.002	2.999±0.081	0.924±0.005	0.513±0.023	0.333±0.014	0.561±0.022
Adsh	113.493 M	13.815 GB	1896 ms	0.035±0.003	3.003±0.111	0.927±0.003	0.511±0.023	0.342±0.011	0.570±0.014
SAW	113.493 M	20.061 GB	1077 ms	0.035±0.002	3.009±0.083	0.925±0.005	0.509±0.025	0.337±0.014	0.565±0.025
FastECG_{r=16}	2.234 M	9.235 GB	530 ms	0.029±0.001	2.779±0.027	0.931±0.002	0.523±0.027	0.344±0.010	0.578±0.013
FastECG_{r=4}	0.740 M	9.223 GB	528 ms	0.028±0.001	2.741±0.039	0.930±0.002	0.513±0.018	0.346±0.007	0.584±0.009
Chapman Dataset									
ReMixMatch	113.487 M	26.324 GB	1406 ms	0.090±0.013	3.391±0.212	0.850±0.007	0.416±0.017	0.265±0.011	0.453±0.021
MixedTeacher	113.487 M	14.257 GB	724 ms	0.040±0.003	2.493±0.077	0.904±0.009	0.544±0.011	0.341±0.007	0.516±0.022
FixMatch	113.487 M	20.061 GB	960 ms	0.042±0.002	2.545±0.048	0.900±0.008	0.534±0.014	0.350±0.013	0.518±0.026
FlexMatch	113.487 M	20.061 GB	937 ms	0.045±0.003	2.620±0.079	0.895±0.014	0.523±0.024	0.333±0.018	0.495±0.025
SoftMatch	113.487 M	20.061 GB	931 ms	0.043±0.003	2.555±0.068	0.894±0.008	0.536±0.011	0.345±0.010	0.518±0.021
Adsh	113.487 M	13.815 GB	957 ms	0.046±0.003	2.649±0.075	0.893±0.009	0.533±0.010	0.341±0.010	0.511±0.014
SAW	113.487 M	20.061 GB	933 ms	0.044±0.004	2.599±0.093	0.900±0.007	0.533±0.011	0.344±0.015	0.518±0.029
FastECG_{r=16}	2.205 M	9.223 GB	451 ms	0.037±0.001	2.417±0.035	0.904±0.004	0.556±0.006	0.371±0.010	0.552±0.018
FastECG_{r=4}	0.716 M	9.206 GB	451 ms	0.036±0.001	2.404±0.041	0.902±0.006	0.550±0.008	0.365±0.006	0.548±0.010

Extended Data Table 5: Performance comparisons between FastECG and parameter-efficient semi-supervised baselines on the medium backbone. The average performance on all CVDs within each dataset is shown across six seeds. The standard deviation is also reported for the evaluation metrics.

Methods	Params ↓	Time/iter ↓	Ranking Loss ↓	Coverage ↓	Macro AUC ↑	MAP ↑	Macro $G_{\beta=2}$ ↑	Macro $F_{\beta=2}$ ↑
G12EC Dataset								
FixMatch	50.493 M	499 ms	0.096±0.006	4.027±0.109	0.850±0.009	0.499±0.014	0.299±0.016	0.529±0.016
+ LoRA _{r=16}	2.135 M	545 ms	0.093±0.003	3.943±0.094	0.854±0.005	0.494±0.006	0.300±0.016	0.534±0.024
+ DyLoRA _{r=16}	2.135 M	542 ms	0.092±0.003	3.913±0.117	0.851±0.007	0.494±0.012	0.296±0.015	0.533±0.021
+ AdaLoRA _{r=16}	2.136 M	585 ms	0.096±0.004	4.013±0.095	0.847±0.008	0.478±0.014	0.296±0.009	0.533±0.008
+ IncreLoRA _{r=16}	2.164 M	977 ms	0.085±0.003	3.683±0.100	0.859±0.007	0.482±0.005	0.299±0.011	0.553±0.014
+ LoRA _{r=4}	0.597 M	543 ms	0.092±0.003	3.895±0.075	0.850±0.007	0.485±0.006	0.292±0.021	0.522±0.021
+ DyLoRA _{r=4}	0.597 M	542 ms	0.093±0.006	3.910±0.159	0.851±0.006	0.483±0.008	0.292±0.017	0.532±0.021
+ AdaLoRA _{r=4}	0.598 M	584 ms	0.093±0.005	3.933±0.135	0.850±0.005	0.486±0.005	0.295±0.008	0.533±0.012
+ IncreLoRA _{r=4}	0.621 M	749 ms	0.084±0.003	3.660±0.114	0.861±0.007	0.486±0.008	0.301±0.007	0.552±0.013
FastECG_{r=16}	1.568 M	243 ms	0.086±0.004	3.740±0.134	0.862±0.006	0.507±0.007	0.317±0.022	0.561±0.024
FastECG_{r=4}	0.458 M	241 ms	0.085±0.002	3.741±0.068	0.862±0.007	0.503±0.006	0.316±0.013	0.560±0.015
PTB-XL Dataset								
FixMatch	50.494 M	553 ms	0.034±0.002	2.767±0.053	0.898±0.003	0.536±0.006	0.340±0.006	0.556±0.010
+ LoRA _{r=16}	2.135 M	603 ms	0.030±0.001	2.632±0.050	0.906±0.005	0.532±0.005	0.352±0.008	0.571±0.012
+ DyLoRA _{r=16}	2.135 M	603 ms	0.031±0.001	2.683±0.060	0.903±0.006	0.533±0.008	0.344±0.017	0.567±0.017
+ AdaLoRA _{r=16}	2.137 M	652 ms	0.031±0.001	2.636±0.022	0.905±0.004	0.529±0.006	0.350±0.006	0.571±0.005
+ IncreLoRA _{r=16}	2.005 M	1090 ms	0.029±0.001	2.567±0.029	0.908±0.004	0.540±0.007	0.364±0.007	0.586±0.013
+ LoRA _{r=4}	0.598 M	602 ms	0.030±0.001	2.609±0.056	0.908±0.005	0.530±0.006	0.345±0.008	0.571±0.013
+ DyLoRA _{r=4}	0.598 M	600 ms	0.030±0.001	2.607±0.038	0.907±0.003	0.530±0.005	0.342±0.022	0.564±0.016
+ AdaLoRA _{r=4}	0.598 M	650 ms	0.030±0.001	2.610±0.024	0.907±0.003	0.534±0.005	0.354±0.003	0.578±0.006
+ IncreLoRA _{r=4}	0.623 M	830 ms	0.028±0.000	2.548±0.009	0.912±0.002	0.542±0.005	0.362±0.013	0.586±0.012
FastECG_{r=16}	1.485 M	271 ms	0.027±0.001	2.539±0.033	0.913±0.003	0.550±0.004	0.369±0.005	0.588±0.003
FastECG_{r=4}	0.505 M	270 ms	0.027±0.001	2.529±0.019	0.914±0.003	0.547±0.003	0.372±0.006	0.599±0.010
Ningbo Dataset								
FixMatch	50.496 M	572 ms	0.031±0.002	2.869±0.081	0.931±0.003	0.531±0.021	0.349±0.014	0.575±0.015
+ LoRA _{r=16}	2.137 M	625 ms	0.028±0.001	2.759±0.044	0.927±0.003	0.518±0.017	0.345±0.008	0.580±0.012
+ DyLoRA _{r=16}	2.137 M	625 ms	0.028±0.002	2.735±0.061	0.928±0.004	0.502±0.022	0.331±0.009	0.564±0.014
+ AdaLoRA _{r=16}	2.139 M	674 ms	0.030±0.001	2.799±0.084	0.927±0.002	0.507±0.020	0.330±0.010	0.565±0.018
+ IncreLoRA _{r=16}	2.145 M	1124 ms	0.027±0.001	2.679±0.044	0.932±0.002	0.521±0.014	0.337±0.008	0.569±0.015
+ LoRA _{r=4}	0.600 M	624 ms	0.028±0.001	2.722±0.058	0.929±0.002	0.516±0.014	0.338±0.015	0.565±0.016
+ DyLoRA _{r=4}	0.600 M	621 ms	0.028±0.001	2.717±0.039	0.929±0.002	0.510±0.018	0.335±0.011	0.569±0.017
+ AdaLoRA _{r=4}	0.600 M	672 ms	0.030±0.003	2.790±0.083	0.927±0.004	0.505±0.019	0.325±0.006	0.558±0.017
+ IncreLoRA _{r=4}	0.622 M	858 ms	0.027±0.001	2.667±0.018	0.931±0.001	0.519±0.013	0.338±0.010	0.569±0.018
FastECG_{r=16}	1.705 M	282 ms	0.027±0.001	2.701±0.051	0.933±0.003	0.531±0.018	0.356±0.013	0.588±0.021
FastECG_{r=4}	0.507 M	282 ms	0.026±0.001	2.661±0.058	0.934±0.004	0.525±0.018	0.352±0.013	0.587±0.020
Chapman Dataset								
FixMatch	50.492 M	495 ms	0.038±0.004	2.439±0.092	0.905±0.010	0.538±0.011	0.357±0.009	0.522±0.020
+ LoRA _{r=16}	2.134 M	540 ms	0.038±0.002	2.424±0.053	0.899±0.009	0.532±0.021	0.345±0.009	0.514±0.024
+ DyLoRA _{r=16}	2.134 M	540 ms	0.037±0.004	2.401±0.095	0.903±0.008	0.531±0.013	0.345±0.013	0.518±0.027
+ AdaLoRA _{r=16}	2.135 M	583 ms	0.037±0.002	2.394±0.066	0.894±0.009	0.511±0.020	0.343±0.004	0.493±0.013
+ IncreLoRA _{r=16}	2.159 M	962 ms	0.035±0.001	2.337±0.034	0.889±0.010	0.515±0.013	0.342±0.011	0.496±0.017
+ LoRA _{r=4}	0.596 M	539 ms	0.036±0.002	2.372±0.051	0.901±0.005	0.535±0.007	0.357±0.010	0.521±0.022
+ DyLoRA _{r=4}	0.596 M	537 ms	0.036±0.002	2.371±0.034	0.903±0.005	0.528±0.015	0.350±0.011	0.515±0.020
+ AdaLoRA _{r=4}	0.597 M	580 ms	0.036±0.002	2.362±0.029	0.901±0.008	0.521±0.018	0.344±0.006	0.508±0.006
+ IncreLoRA _{r=4}	0.618 M	746 ms	0.035±0.002	2.348±0.046	0.888±0.010	0.510±0.016	0.344±0.008	0.502±0.020
FastECG_{r=16}	1.601 M	241 ms	0.035±0.002	2.362±0.049	0.909±0.007	0.553±0.013	0.367±0.008	0.540±0.019
FastECG_{r=4}	0.402 M	240 ms	0.034±0.001	2.334±0.033	0.908±0.008	0.538±0.014	0.361±0.009	0.531±0.019

Extended Data Table 6: Performance comparisons between FastECG and parameter-efficient semi-supervised baselines on the large backbone. The average performance on all CVDs within each dataset is shown across six seeds. The standard deviation is also reported for the evaluation metrics.

Methods	Params ↓	Time/iter ↓	Ranking Loss ↓	Coverage ↓	Macro AUC ↑	MAP ↑	Macro $G_{\beta=2}$ ↑	Macro $F_{\beta=2}$ ↑
G12EC Dataset								
FixMatch	113.489 M	966 ms	0.100±0.005	4.147±0.113	0.843±0.007	0.493±0.008	0.293±0.011	0.518±0.015
+ LoRA _{r=16}	3.201 M	1023 ms	0.094±0.003	3.983±0.134	0.849±0.004	0.492±0.006	0.294±0.010	0.530±0.020
+ DyLoRA _{r=16}	3.201 M	1024 ms	0.091±0.003	3.911±0.070	0.849±0.005	0.492±0.008	0.297±0.017	0.534±0.022
+ AdaLoRA _{r=16}	3.203 M	1025 ms	0.093±0.003	3.972±0.119	0.842±0.003	0.482±0.008	0.296±0.008	0.532±0.010
+ InceLoRA _{r=16}	3.245 M	1575 ms	0.084±0.002	3.708±0.075	0.851±0.003	0.493±0.008	0.309±0.013	0.543±0.021
+ LoRA _{r=4}	0.896 M	1021 ms	0.092±0.005	3.895±0.130	0.851±0.005	0.493±0.007	0.296±0.010	0.530±0.012
+ DyLoRA _{r=4}	0.896 M	1021 ms	0.090±0.004	3.864±0.133	0.849±0.006	0.495±0.008	0.301±0.010	0.535±0.008
+ AdaLoRA _{r=4}	0.896 M	1021 ms	0.089±0.002	3.852±0.069	0.847±0.004	0.487±0.003	0.297±0.018	0.527±0.024
+ InceLoRA _{r=4}	0.921 M	1348 ms	0.082±0.003	3.666±0.086	0.856±0.006	0.497±0.007	0.308±0.010	0.542±0.016
FastECG_{r=16}	2.658 M	453 ms	0.085±0.005	3.778±0.140	0.857±0.004	0.509±0.007	0.322±0.009	0.565±0.010
FastECG_{r=4}	0.761 M	453 ms	0.084±0.003	3.742±0.117	0.859±0.004	0.506±0.007	0.323±0.004	0.561±0.002
PTB-XL Dataset								
FixMatch	113.490 M	1072 ms	0.035±0.003	2.805±0.102	0.894±0.004	0.521±0.006	0.342±0.007	0.560±0.012
+ LoRA _{r=16}	3.202 M	1135 ms	0.030±0.001	2.635±0.023	0.903±0.002	0.522±0.006	0.332±0.010	0.550±0.014
+ DyLoRA _{r=16}	3.202 M	1135 ms	0.031±0.001	2.674±0.030	0.906±0.002	0.528±0.002	0.346±0.010	0.566±0.008
+ AdaLoRA _{r=16}	3.203 M	1138 ms	0.033±0.000	2.716±0.019	0.894±0.003	0.517±0.006	0.345±0.008	0.558±0.006
+ InceLoRA _{r=16}	3.167 M	1758 ms	0.031±0.001	2.660±0.030	0.898±0.004	0.519±0.004	0.348±0.012	0.566±0.012
+ LoRA _{r=4}	0.897 M	1133 ms	0.030±0.001	2.621±0.026	0.904±0.003	0.523±0.006	0.342±0.012	0.564±0.014
+ DyLoRA _{r=4}	0.897 M	1133 ms	0.030±0.001	2.632±0.030	0.903±0.004	0.525±0.004	0.339±0.011	0.570±0.010
+ AdaLoRA _{r=4}	0.897 M	1134 ms	0.032±0.001	2.699±0.052	0.897±0.004	0.516±0.004	0.339±0.007	0.567±0.007
+ InceLoRA _{r=4}	0.920 M	1493 ms	0.030±0.000	2.631±0.016	0.901±0.002	0.524±0.005	0.351±0.005	0.573±0.010
FastECG_{r=16}	2.235 M	508 ms	0.030±0.002	2.618±0.061	0.909±0.004	0.537±0.004	0.358±0.005	0.587±0.008
FastECG_{r=4}	0.712 M	506 ms	0.029±0.001	2.602±0.028	0.908±0.003	0.535±0.004	0.356±0.006	0.582±0.008
Ningbo Dataset								
FixMatch	113.493 M	1111 ms	0.033±0.002	2.962±0.070	0.926±0.004	0.513±0.024	0.337±0.018	0.563±0.027
+ LoRA _{r=16}	3.205 M	1177 ms	0.030±0.002	2.845±0.073	0.925±0.003	0.508±0.023	0.336±0.009	0.566±0.017
+ DyLoRA _{r=16}	3.205 M	1176 ms	0.030±0.002	2.834±0.093	0.927±0.003	0.504±0.024	0.326±0.013	0.553±0.019
+ AdaLoRA _{r=16}	3.206 M	1180 ms	0.031±0.001	2.855±0.074	0.920±0.002	0.491±0.017	0.315±0.011	0.545±0.018
+ InceLoRA _{r=16}	3.247 M	1766 ms	0.028±0.001	2.750±0.030	0.926±0.004	0.502±0.024	0.330±0.009	0.562±0.017
+ LoRA _{r=4}	0.900 M	1173 ms	0.029±0.001	2.802±0.053	0.925±0.002	0.510±0.023	0.332±0.010	0.563±0.018
+ DyLoRA _{r=4}	0.900 M	1174 ms	0.030±0.001	2.803±0.035	0.926±0.003	0.505±0.028	0.330±0.010	0.564±0.020
+ AdaLoRA _{r=4}	0.900 M	1175 ms	0.031±0.003	2.846±0.128	0.922±0.002	0.495±0.023	0.326±0.012	0.555±0.023
+ InceLoRA _{r=4}	0.923 M	1545 ms	0.028±0.001	2.736±0.028	0.927±0.003	0.499±0.016	0.329±0.011	0.561±0.017
FastECG_{r=16}	2.234 M	530 ms	0.029±0.001	2.779±0.027	0.931±0.002	0.523±0.027	0.344±0.010	0.578±0.013
FastECG_{r=4}	0.740 M	528 ms	0.028±0.001	2.741±0.039	0.930±0.002	0.513±0.018	0.346±0.007	0.584±0.009
Chapman Dataset								
FixMatch	113.487 M	960 ms	0.042±0.002	2.545±0.048	0.900±0.008	0.534±0.014	0.350±0.013	0.518±0.026
+ LoRA _{r=16}	3.200 M	1016 ms	0.040±0.003	2.501±0.079	0.896±0.004	0.541±0.005	0.343±0.015	0.509±0.024
+ DyLoRA _{r=16}	3.200 M	1016 ms	0.040±0.004	2.484±0.080	0.897±0.006	0.537±0.009	0.352±0.006	0.524±0.021
+ AdaLoRA _{r=16}	3.201 M	1018 ms	0.037±0.002	2.416±0.039	0.894±0.003	0.531±0.011	0.343±0.011	0.509±0.021
+ InceLoRA _{r=16}	3.231 M	1541 ms	0.033±0.002	2.309±0.037	0.895±0.008	0.539±0.014	0.355±0.010	0.517±0.017
+ LoRA _{r=4}	0.894 M	1016 ms	0.038±0.001	2.452±0.039	0.901±0.006	0.542±0.008	0.338±0.015	0.512±0.028
+ DyLoRA _{r=4}	0.894 M	1015 ms	0.037±0.003	2.415±0.068	0.899±0.005	0.533±0.015	0.341±0.013	0.505±0.021
+ AdaLoRA _{r=4}	0.895 M	1015 ms	0.036±0.001	2.412±0.039	0.898±0.005	0.543±0.007	0.341±0.007	0.517±0.019
+ InceLoRA _{r=4}	0.920 M	1340 ms	0.033±0.001	2.316±0.028	0.897±0.007	0.539±0.025	0.360±0.017	0.528±0.019
FastECG_{r=16}	2.205 M	451 ms	0.037±0.001	2.417±0.035	0.904±0.004	0.556±0.006	0.371±0.010	0.552±0.018
FastECG_{r=4}	0.716 M	451 ms	0.036±0.001	2.404±0.041	0.902±0.006	0.550±0.008	0.365±0.006	0.548±0.010